CR-165503
PWA 5779-10

NASA-CR-165503
19820015374

NASA

ANALYSIS OF HIGH LOAD DAMPERS

Final Report

by

S. T. Bhat, D. F. Buono, and D. H. Hibner

United Technologies Corporation
Pratt & Whitney Aircraft Group
Commercial Products Division

Prepared for

National Aeronautics and Space Administration
Lewis Research Center
Contract NAS3-22518

UNITED TECHNOLOGIES
PRATT&WHITNEY
AIRCRAFT

400 Main Street
East Hartford, Connecticut 06108

Commercial Products Division

In reply please refer to:
DHH:JK:jk - Eng. 3S3
PWA-5779-10

30 April 1982

To: National Aeronautics and Space Administration
Lewis Research Center
21000 Brookpark Road
Cleveland, Ohio 44135

Attention: Mr. Alexis W. Puher
Contracting Officer

Subject: Submittal of the Final Report (CR-165503):
"Analysis of High Load Dampers"

Reference: (1) Contract NAS3-22518
(2) NASA Lewis Letter 1430, B. F. Robinson to
D. H. Hibner, dated 5 November 1981

Gentlemen:

We submit herewith the Contractor Final Report (CR-165503) for the subject program in compliance with the reporting requirements of the Reference (1) contract. NASA approval for final submittal of this report, contingent on incorporation of the revisions and corrections specified by NASA, was received via the Reference (2) letter. Additional distribution of this report is being made in accordance with the distribution list supplied by NASA.

Sincerely yours,

UNITED TECHNOLOGIES CORPORATION
Pratt & Whitney Aircraft Group
Commercial Products Division

D. H. Hibner
Program Manager

1.REPORT NO. NASA CR-165503	2. GOVERNMENT AGENCY	3.RECIPIENT'S CATALOG NO.
4.TITLE AND SUBTITLE Analysis of High Load Dampers		5. REPORT DATE 21 August 1981 6. PERFORMING ORG. CODE
7.AUTHOR(S) S. T. Bhat, D. F. Buono, D. H. Hibner		8. PERFORMING ORG. REPT. NO. PWA-5779-10
9.PERFORMING ORG. NAME AND ADDRESS United Technologies Corporation Pratt & Whitney Aircraft Group Commercial Products Division		10. WORK UNIT NO. 11. CONTRACT OR GRANT NO. NAS3-22518
12. SPONSORING AGENCY NAME AND ADDRESS National Aeronautics and Space Administration Washington, D.C. 20516		13. TYPE REPT./PERIOD COVERED Contractor Report 14. SPONSORING AGENCY CODE

15. SUPPLEMENTARY NOTES

Project Manager, Dr. David P. Fleming, Structures and Mechanical Technologies Division, NASA Lewis Research Center, Cleveland, Ohio 44135

16. ABSTRACT

This program focused on the definition of high load damping requirements for modern jet engines, and the evaluation, selection, and design of damping systems which could satisfy these requirements. In order to evaluate high load damping requirements, engines in three major classes were studied; large transport engines, small general aviation engines, and military engines. Four damper concepts applicable to these engines were evaluated; multi-ring, cartridge, curved beam, and viscous/friction. The most promising damper concept was selected for each engine and performance was assessed relative to conventional dampers and in light of projected damping requirements for advanced jet engines.

17. KEY WORDS (SUGGESTED BY AUTHOR(S))	18. DISTRIBUTION STATEMENT
Rotor Dynamics High Load Dampers Gas Turbine Engines Squeeze Film Dampers	

19. SECURITY CLASS (THIS REPT)	20. SECURITY CLASS (THIS PAGE)	21. NO. PGS	22. PRICE *
Unclassified	Unclassified		

* For sale by the National Technical Information Service, Springfield, VA 22161

FOREWORD

This report documents a contracted study of high load damper systems conducted for NASA by Pratt & Whitney Aircraft. This study was conducted under NASA Contract NAS3-22518.

The NASA Technical Manager for this study contract was Dr. David P. Fleming, Lewis Research Center, Cleveland, Ohio. Key Pratt & Whitney Aircraft personnel were David H. Hibner, Study Program Manager, Shrikant T. Bhat, and Dennis F. Buono, Major Technical Contributors.

TABLE OF CONTENTS

Section	Title	Page
1.0	SUMMARY	1
2.0	INTRODUCTION	3
3.0	ENGINE MODELS AND DAMPER CONCEPTS	5
	3.1 Engine Models	5
	3.1.1 Large Transport Engines	5
	3.1.2 Small General Aviation Engines	7
	3.1.3 Military Engines	9
	3.2 Damper Concepts	11
	3.2.1 Multi-Ring Damper	12
	3.2.2 Cartridge Damper	13
	3.2.3 Curved Beam Damper	13
	3.2.4 Viscous/Friction Damper	15
4.0	ANALYTICAL METHODS	17
	4.1 Critical Speed Analysis	17
	4.1.1 Large Transport Engine	19
	4.1.1.1 Low Rotor Excited Modes	19
	4.1.1.2 High Rotor Excited Modes	22
	4.1.2 Small General Aviation Engine	23
	4.1.3 Military Engine	25
	4.1.3.1 Low Rotor Excited Modes	25
	4.1.3.2 High Rotor Excited Modes	28
	4.2 Forced Response Analysis	29
	4.2.1 Large Transport Engine	29
	4.2.2 Small General Aviation Engine	32
	4.2.3 Military Engine	35
	4.3 Damper Analysis	37
	4.3.1 Multi-Ring Damper	38
	4.3.2 Cartridge Damper	42
	4.3.3 Curved Beam Damper	43
	4.3.4 Viscous/Friction Damper	45

TABLE OF CONTENTS (continued)

Section	Title	Page
5.0	RESULTS AND DISCUSSION OF RESULTS	47
	5.1 Damper Operating Requirements	47
	5.1.1 Large Transport Engine	48
	5.1.2 Small General Aviation Engine	49
	5.1.3 Military Engine	50
	5.2 Selected Damper Concepts	51
	5.2.1 Large Transport Engine	52
	5.2.2 Small General Aviation Engine	54
	5.2.3 Military Engine	55
	5.3 Predicted Performance	56
	5.3.1 Large Transport Engine	56
	5.3.2 Small General Aviation Engine	60
	5.3.3 Military Engine	63
6.0	CONCLUSIONS AND RECOMMENDATIONS	67
REFERENCES		69
NOMENCLATURE		71
DISTRIBUTION LIST		73

LIST OF TABLES

Number	Title	Page
3.1-I	Assumed Stiffnesses for Large Transport Engine Bearings	7
3.1-II	Assumed Stiffnesses for Small General Aviation Engine Bearings	9
3.1-III	Assumed Stiffnesses for Military Engine Bearings	11
4.3-I	Stiffness and Damping Expressions for Short Bearing and Long Bearing Approximations	38
5.1-I	High and Low Load Damping Limits, Damper Requirements, and Expected Engine Response at High and Low Loads	51
5.2-I	Damper Geometry and Operating Conditions	53
5.3-I	Large Transport Engine Response; Proposed Damper (29 mil, Parallel Supported Damper)	59
5.3-II	Large Transport Engine Response; Conventional Squeeze Film Damper (5 mil Damper)	59
5.3-III	Small General Aviation Engine Response; Proposed Damper (Curved Beam)	62
5.3-IV	Small General Aviation Engine Response; Conventional Damper (5 mil Squeeze Film)	62
5.3-V	Military Engine Response; Proposed Damper (Curved Beam)	65
5.3-VI	Military Engine Response; Conventional Damper (5 mil Squeeze Film)	65

LIST OF ILLUSTRATIONS

Number	Title	Page
3.1-1	Line Diagram for the Large Transport Engine Model	7
3.1-2	Line Diagram for the Small General Aviation Engine Model	8
3.1-3	Line Diagram for the Military Engine Model	10
3.2-1	Multi-Ring Damper Concept	13
3.2-2	Cartridge Damper Concept	14
3.2-3	Curved Beam Damper Concept	14
3.2-4	Viscous/Friction Damper Concept	15
4.1-1	Low Rotor Critical Speed Mode Shapes and Energy Distribution; Large Transport Engine	20
4.1-2	High Rotor Critical Speed Mode Shapes and Energy Distribution; Large Transport Engine	21
4.1-3	Critical Speed Mode Shapes and Energy Distribution; Small General Aviation Engine	24
4.1-4	Low Rotor Critical Speed Mode Shapes and Energy Distribution; Military Engine	26
4.1-5	High Rotor Critical Speed Mode Shapes and Energy Distribution; Military Engine	27
4.2-1	Critical Mode Shape (Rotor Only); Imbalance Location and Critical Response Locations; Large Transport Engine	29
4.2-2	Fifth Stage Compressor Gap Reduction Sensitivity; Large Transport Engine	31
4.2-3	Number 2 Bearing Support Load Sensitivity; Large Transport Engine	31
4.2-4	Support Deflection Response Sensitivities; Large Transport Engine	32
4.2-5	Critical Mode Shape (Rotor Only); Imbalance Location and Critical Deflection Locations; Small General Aviation Engine	32

LIST OF ILLUSTRATIONS (continued)

Number	Title	Page
4.2-6	Second Stage Turbine Gap Reduction Sensitivity; Small General Aviation Engine	33
4.2-7	Number 3 Bearing Support Load Sensitivity; Small General Aviation Engine	34
4.2-8	Support Deflection Response Sensitivities; Small General Aviation Engine	34
4.2-9	Critical Mode Shape (Rotor Only); Imbalance Location and Critical Deflection Locations; Military Engine	35
4.2-10	First Stage Turbine Gap Reduction Sensitivity; Military Engine	36
4.2-11	Number 5 Bearing Support Load Sensitivity; Military Engine	36
4.2-12	Support Deflection Response Sensitivities; Military Engine	37
4.3-1	Geometric Arrangement of a Two-Film Damper	39
4.3-2	Stiffness and Damping Coefficients; Single Film and Multi-Ring Dampers	41
4.3-3	Comparison of Stiffness and Damping Coefficients; Cartridge Damper and Conventional Squeeze Film Damper	42
4.3-4	Curved Beam Damper Geometry	43
5.3-1	Compressor Gap Reduction at Low, Intermediate, and High Levels of Imbalance; Conventional and Proposed Dampers; Large Tranport Engine	57
5.3-2	Number 2 Bearing Loads; Conventional and Proposed Dampers; Large Transport Engine	58
5.3-3	Turbine Gap Reduction at Low, Intermediate, and High Levels of Imbalance; Conventional and Proposed Dampers; Small General Aviation Engine	60
5.3-4	Number 3 Bearing Loads; Conventional and Proposed Dampers; Small General Aviation Engine	61
5.3-5	Turbine Gap Reduction at Low, Intermediate, and High Levels of Imbalance; Conventional and Proposed Dampers; Military Engine	63
5.3-6	Number 5 Bearing Loads; Conventional and Proposed Dampers; Military Engine	64

SECTION 1.0

SUMMARY

This program focused on the definition of high load damping requirements for modern jet engines, and the evaluation, selection and design of damping systems which could satisfy these requirements. In order to evaluate high load damping requirements, engines representative of three classes of modern gas turbines were studied; large transport engines, small general aviation engines, and military engines. Four damper concepts applicable to these engines were evaluated; multi-ring squeeze film damper, cartridge squeeze film damper, curved beam damper, and a combination viscous (squeeze film)/friction damper. The most promising damper concept was selected for each engine and performance was assessed relative to conventional dampers and relative to projected damping requirements for advanced jet engines.

A hypothetical representative engine model was specified for each of the three engine classes, and damping requirements for one sensitive rotor bending mode for each engine were investigated. Mode selection was based on sensitivity to imbalance and the probability of being subject to a high imbalance load condition. The military and small general aviation engines were found to have a sensitive turbine mode within the operating range, while the large transport engine had a high compressor bending mode. Maximum imbalance was based on the loss of a single airfoil blade in the turbine or compressor, as applicable. The highest imbalance was of the order of 3600 gm-cm for both the military and large transport engines, and 720 gm-cm for the small general aviation engine. Selection of required damper characteristics to control each mode was based on meeting allowable rotor-to-case gap reductions and bearing loads.

Four damper concepts were evaluated in the study. A preliminary review was conducted to determine whether they could be designed to supply the damping and stiffness required to control the specified mode for each engine. As a result of this analysis, two concepts were selected for application to the representative engines. The curved beam damper was chosen for the military and small general aviation engines due to its linearity and compactness. A conventional closed ended squeeze film damper with a large clearance and parallel spring support was selected for the large transport engine. The large bearing size in this type of engine allows sufficient stiffness and damping coefficients with reasonable oil film dimensions.

The performance of the selected damper concepts was assessed analytically, based on predicted vibration loads and deflections for the representative engines. The dampers were sized to meet the high load damping requirements for each engine, and forced response analysis models which included rotors and case structures were developed. Steady state forced response analyses were conducted for each engine, covering the range of imbalance from normal residual to the most severe. The predicted response with the high load dampers was compared to the response with conventional squeeze film dampers designed for normal residual imbalance only. The high load dampers performed well in their respective applications, maintaining engine loads and deflections within required limits. The conventional squeeze film dampers could not control high imbalance loads in the representative engines.

The major conclusions drawn from this study are as follows:

- Conventional squeeze film dampers designed for normal residual imbalance are too nonlinear to function well under high imbalance load conditions.

- The curved beam damper showed the greatest potential for successful application in future engines due to its linearity and independent control of stiffness and damping.

SECTION 2.0

INTRODUCTION

The higher thrusts and greater efficiencies of advanced jet engines require higher operating speeds and more flexible rotors and case structures. This advance in engine development puts a greater emphasis on rotor vibration and associated loads and deflections. The higher speeds and lighter, more flexible structures result in rotor natural frequencies which are below maximum rotor speeds. In addition, loads and deflections caused by rotor imbalance are increased because of higher speeds and resonance effects.

Squeeze film dampers have been used effectively in past and current gas turbine engines to control vibration caused by residual rotor imbalance. The capability of these devices to attenuate the relatively low levels of vibrational energy caused by residual rotor imbalance has been demonstrated in both theory and experience. However, these dampers are not designed to handle unusual and severe imbalances.

Squeeze film dampers have inherent theoretical and practical limitations which reduce their effectiveness in handling a high imbalance load such as that which might be produced by blade damage from bird or foreign object ingestion. The forces produced by a squeeze film damper are highly nonlinear and increase rapidly as the damper excursion, which is dependent on imbalance, becomes large. Thus, to produce high damping forces, a squeeze film damper must theoretically operate at very high eccentricities. With this constraint, effectiveness is seriously impaired by the following:

- Surface to surface contact can occur in the damper, thereby disrupting the hydrodynamic film and therefore altering stiffness and damping forces.

- Stiffness of the oil film increases rapidly, a situation which allows more of the vibrational energy to be transferred to the static structure, i.e., high transmissibility.

- Oil leakage past the seals can reduce damper load capacity significantly below predicted levels.

The requirements placed on a damper to control high load vibration modes are functions not only of the load level and type of mode but also the type of engine and the mission it is expected to complete. Commercial transport engines have the highest imbalances during blade loss due to their large fan and turbine blades. However, these engines may not need to continue running under such high loads because the plane may land safely using the remaining engines. The situation is different with military engines; smaller than the commercial engines and with generally lower vibration loads, continued operation of these engines for limited periods may be necessary under high imbalance load conditions. Finally, small general aviation engines are subjected to lower imbalances because of their smaller rotor and airfoil sizes. Yet, high operating speeds produce high loads, and the lighter and softer engine case and support structures have limited load carrying capabilities.

This program was designed to add to the technology base which will be used to develop dampers for modern gas turbine engines which are subject to high imbalance loads. The dynamic characteristics of three major classes of modern jet engines were defined and damping systems were developed to control engine vibration response under high and low imbalance loads.

Section 3.0 of this report describes the characteristics of the representative engines and the basic features of the damper concepts which were evaluated.

Section 4.0 provides detailed information on the analytical methods and results used in this study.

Section 5.0 contains a discussion of the damping requirements for each engine and an assessment of the performance of the selected damper concepts.

Section 6.0 presents conclusions from this study and recommendations for additional effort in the analysis of high load dampers.

SECTION 3.0

ENGINE MODELS AND DAMPER CONCEPTS

Advanced jet engines will be used for a wide variety of applications, including small commuter aircraft, high performance fighter planes, and large-scale commercial transports. The engines developed for these applications will differ in design philososphy, operating conditions, and susceptibility to in-flight problems. However, due to the world fuel situation, higher thrust and greater efficiency will be common requirements for all advanced engines. One important step toward meeting these requirements is the development of lightweight, flexible rotor systems capable of operating at higher speeds than current designs. These advanced rotor systems will be subject to high load vibration conditions unlike those encountered in current engines.

In order to evaluate high load damping requirements for advanced jet engines, analytical models were developed for three major engine classes: small general aviation engines, military turbojets and turbofans, and large transport turbofans. The models for these representative high-technology engines were modified to establish a sensitive vibration mode, where loads and deflections due to rotor imbalance are likely to exceed design limits, within the operating range of each engine. Four high load damping concepts (multi-ring, cartridge, curved beam, and viscous/friction) were evaluated. Each concept offered the potential to effectively control engine vibration response to high imbalance loads.

3.1 ENGINE MODELS

In order to predict high load vibration response, an analytical model was developed for each major class of advanced engine. Three Pratt & Whitney Aircraft engines were used as the basis for these models. The representative engine in each class was modified to establish a sensitive vibration mode within the operating speed range. The resulting sensitive mode was used to evaluate the high load damping requirements for each class of engine and to develop solutions to the high load vibration problem. The modifications made for each model consisted of changes to rotor mass and stifness as well as shifts of operating speed range to reflect advanced higher speed engines.

In this section, a line diagram is used to illustrate the key features of each engine model. The line diagram shows the rotors and static cases, as well as various support locations between rotating and nonrotating structures. Each line in the diagram consists of lumped masses representing disks, blades, supports, and rotors, connected by massless springs which represent rotor, stator, and support stiffnesses.

3.1.1 Large Transport Engines

Engines in this class are generally dual-rotor high bypass ratio turbofans with thrust ratings in the 88,960 N to 270,000 N (20,000 to 60,000 lbs) range and operating speeds of less than 20,000 rpm. The Commercial Products Division

of Pratt & Whitney Aircraft has designed and built thousands of these powerplants for large scale commercial transports, including JT8D and JT9D engines. Large transport turbofans have the highest imbalances during blade loss due to their large fans and turbines. Safe shutdown following blade loss or foreign object damage is considered the key criterion for this class of engine.

The model used to represent an advanced large scale transport engine is a modified dual-rotor turbofan with the following characteristics:

Type of Engine:	Dual Spool Turbofan
Thrust:	222,000 N (50,000 lb)
Speed:	Low Rotor 1000 - 3800 rpm High Rotor 4700 - 8500 rpm
Dimensions:	Length 394 cm (155 in) Diameter 244 cm (96 in)
Number of Stages:	Fan 1 Low Compressor 4 High Compressor 11 High Turbine 2 Low Turbine 4
Low Rotor Weight:	1040 kg (2300 lb)
High Rotor Weight:	590 kg (1300 lb)
Engine Weight:	4080 kg (9000 lb)

The line diagram for the large transport engine model is presented in Figure 3.1-1. The low rotor for this model includes the fan, low pressure compressor and the low pressure turbine. It is approximately 330 cm (130 in) long and supported on two bearings. The high rotor consists of the high pressure compressor and the high pressure turbine. It measures 165 cm (65 in) and is supported on two bearings. The assumed stiffnesses for all four bearings are listed in Table 3.1-I. As shown in the line diagram, the large transport engine was modeled as a six line system for critical speed and forced response analyses.

In order to evaluate high load damping requirements for advanced transport engines, a high compressor vibration mode was brought within the operating range of the model. This mode is sensitive to compressor blade loss, which could result from foreign object damage. Rotor deflections and bearing loads resulting from compressor blade loss could exceed the limits established for safe shutdown of the engine. The shape of the high compressor vibration mode, the critical speed at which it occurs, and the energy distribution through the rotor are described in detail in Section 4.1.1.

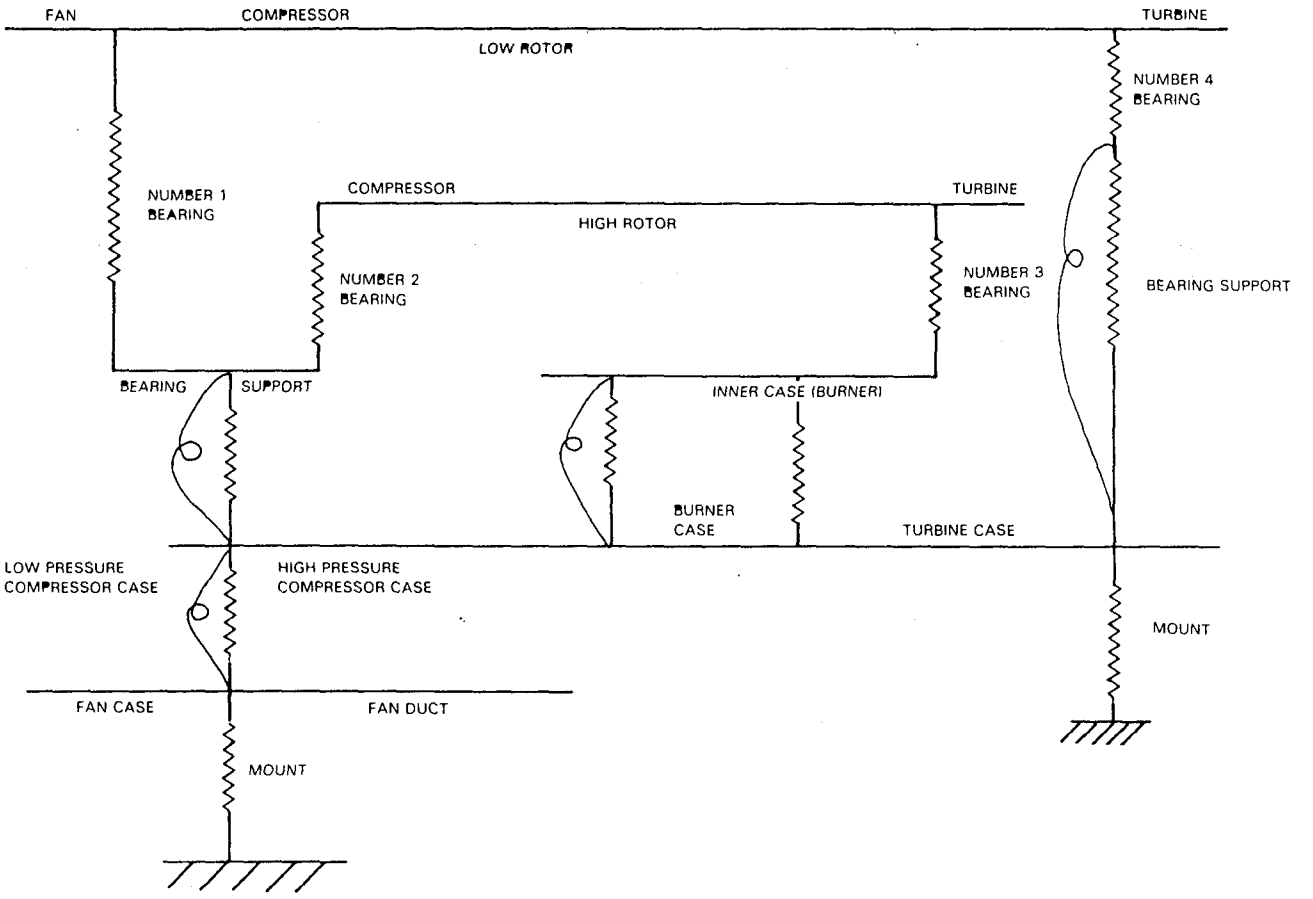

Figure 3.1-1 Line Diagram for Large Transport Engine Model

Table 3.1-I

Assumed Stiffnesses for Large Transport Engine Bearings

Bearing Number	Type	Location	Assumed Stiffness
1	Ball	Low Rotor	390 MN/m (2.2×10^6 lb/in)
2	Ball	High Rotor	310 MN/m (1.76×10^6 lb/in)
3	Roller	High Rotor	160 MN/m (9.2×10^5 lb/in)
4	Roller	Low Rotor	150 MN/m (8.5×10^5 lb/in)

3.1.2 Small General Aviation Engines

This class of engines includes turbojets and turbofans with a thrust rating up to 88,960 N (20,000 lbs) and operating speeds of 20,000 rpm or more. Typical engines in this category are the JT12 and JT15D, manufactured by the

Commercial Products Division of Pratt & Whitney Aircraft and Pratt & Whitney Aircraft of Canada, respectively. Due to their smaller rotor and airfoil size, general aviation engines are subjected to lower imbalances than military and commercial transport engines. However, their higher operating speeds produce high loads, and their lighter and softer engine cases and support structures have limited load carrying capacities. As with large transport engines, safe shutdown following blade loss or foreign object damage is the key criterion for small general aviation engines.

The model used to represent advanced general aviation engines is a modified single spool turbojet with the following characteristics:

Type of Engine:	Single Spool Turbojet
Thrust Rating:	13340 N (3000 lb)
Speed:	9000 - 20,000 rpm
Dimensions:	Length 178 cm (70 in) Diameter 56 cm (22 in)
Number of Stages:	Compressor 9 Turbine 2
Rotor Weight:	70 kg (150 lb)
Engine Weight:	200 kg (450 lb)

The line diagram for the small general aviation engine model is shown in Figure 3.1-2. The rotor, which includes the compressor and turbine, is approximately 127 cm (50 in) long and supported on three bearings (see Table 3.1-II). This engine was modeled as a two line system for dynamic analyses.

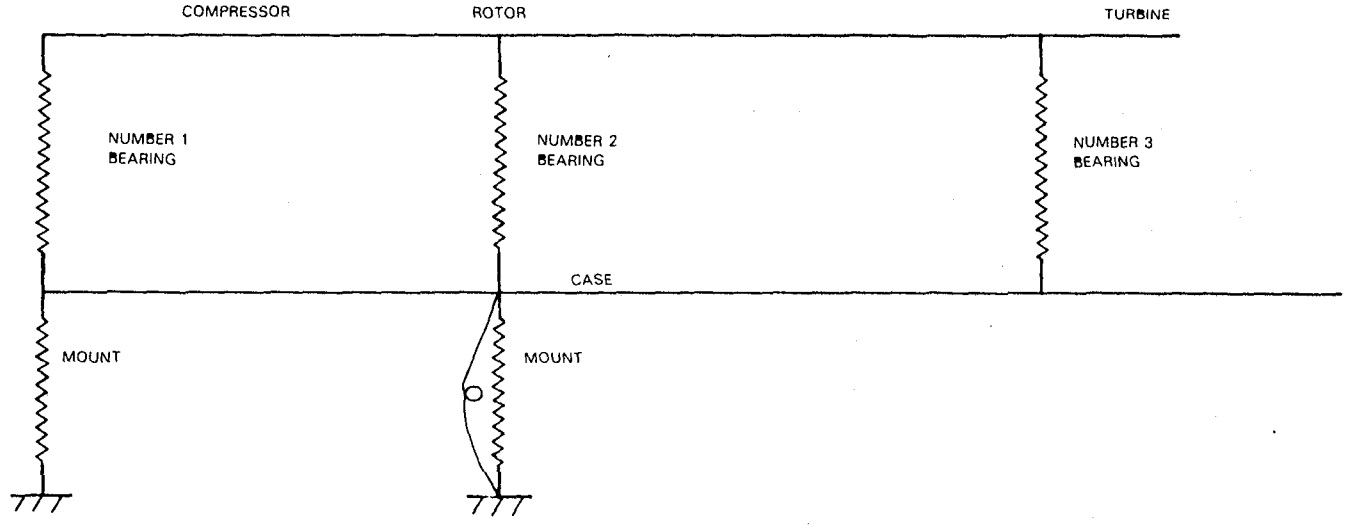

Figure 3.1-2 Line Diagram for the Small General Aviation Engine Model

Table 3.1-II

Assumed Stiffnesses for Small General Aviation Engine Bearings

Bearing Number	Type	Assumed Stiffness
1	Roller	64 MN/m (3.64×10^5 lb/in)
2	Ball	43 MN/m (2.45×10^5 lb/in)
3	Roller	28 MN/m (1.6×10^5 lb/in)

In order to evaluate high load damping requirements for advanced general aviation engines, a turbine vibration mode was brought within the operating range of the model. This modification was based on experience which indicates that these engines could be susceptible to turbine blade loss if the mode were within the high speed range. Although the severity of engine vibration depends on several factors (turbine stage, speed at which the blade is released, and proximity of the sensitive mode), bearing loads and blade deflections are likely to exceed design limits following blade loss at the critical speed. The shape of the turbine vibration mode, the critical speed at which it occurs, and the energy distribution through the rotor are described in detail in Section 4.1.2.

3.1.3 Military Engines

This class comprises turbojets and turbofans used in high performance military aircraft. Thrust ratings range from 44,480 N to 133,450 N (10,000 to 30,000 lbs) and operating speeds are generally 20,000 rpm or less. The Government Products Division of Pratt & Whitney Aircraft has manufactured a large number of military engines, including the J57, J75, TF30, TF33 and F100. Because military aircraft are often powered by a single engine, continued operation under high imbalance loads is the key criterion in evaluating damper capability.

The model used to represent advanced military engines is a dual spool turbofan with the following characteristics:

Type of Engine:	Turbofan with Augmentor
Thrust Rating:	11,200 N (25,000 lb)
Speed:	Low Rotor 4700 - 11,500 rpm High Rotor 8800 - 14,700 rpm
Dimensions:	Length 485 cm (191 in) Diameter 117 cm (46 in)

Number of Stages:	Fan	3
	High Compressor	10
	High Turbine	2
	Low Turbine	2
Low Rotor Weight:	160 kg (360 lb)	
High Rotor Weight:	200 kg (440 lb)	
Engine Weight:	1360 kg (3000 lb)	

The line diagram for the military engine model is shown in Figure 3.1-3. In this model, the low rotor includes the fan and low pressure turbine. It is 205 cm (80 in) long and supported on three bearings. The high rotor consists of the high pressure compressor and high pressure turbine. It is 114 cm (45 in) long and supported on two bearings. The assumed stiffnesses for all five bearings are listed in Table 3.1-III. As shown in the diagram, the military engine was modeled as a five line system for dynamic analyses.

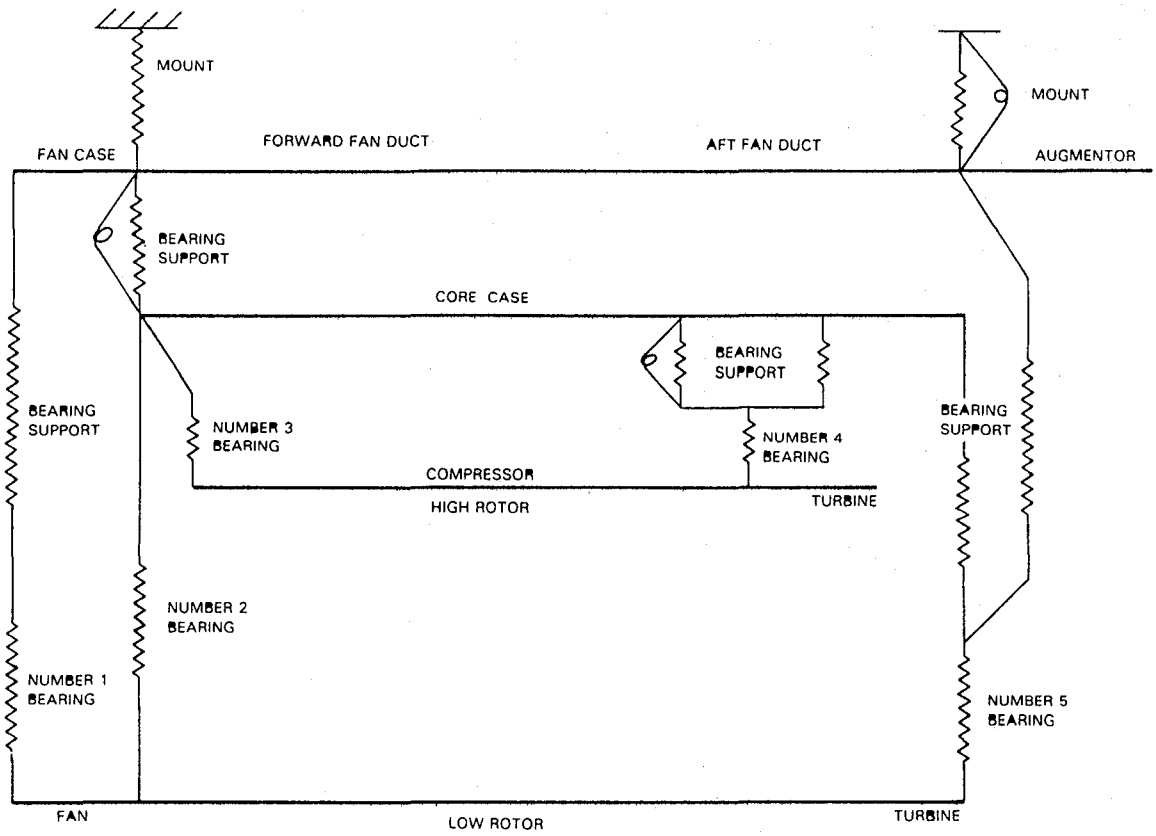

Figure 3.1-3 Line Diagram for the Military Engine Model

Table 3.1-III

Assumed Stiffnesses for Military Engine Bearings

Bearing Number	Type	Location	Assumed Stiffness
1	Roller	Low Rotor	88 MN/m (5.0×10^5 lb/in)
2	Ball	Low Rotor	210 MN/m (1.2×10^6 lb/in)
3	Ball	High Rotor	65 MN/m (3.7×10^5 lb/in)
4	Roller	High Rotor	470 MN/m (2.7×10^6 lb/in)
5	Roller	Low rotor	88 MN/m (5.0×10^5 lb/in)

In order to evaluate high load damping requirements for this advanced military engine, a low turbine vibration mode was brought within the operating range of the model. This mode is sensitive to low turbine blade loss which experience shows could be produced by foreign object damage or component failure (e.g., combustor liner or fatigue failure due to general erosion and higher than anticipated vibratory stress). Because of the design of the representative engine, this incidence of blade loss could cause severe vibration, leading to structural failure. The shape of the low turbine vibration mode, the critical speed at which it occurs, and the energy distribution through the rotor are described in detail in Section 4.1.3.

3.2 DAMPER CONCEPTS

Four advanced damper concepts appear to have the potential to control rotor vibration in tomorrow's jet engines. These designs provide a significant improvement in high load damping capability relative to conventional squeeze film dampers:

- Multi-Ring Damper - Several small clearance squeeze film dampers separated by thin rings provide a higher load-carrying capacity than a single film damper with the same total clearance.
- Cartridge Damper - Use of a sealed unit allows fluid viscosity and supply pressure to be adjusted to specific engine requirements.
- Curved Beam Damper - Curved springs or beams provide constant radial stiffness and constant viscous damping over the entire operating range.
- Viscous/Friction Damper - Annular friction plates operating in series with a conventional squeeze film damper provide flexibility in meeting low and high load damping requirements.

Conventional dampers have been proven to be very effective in controlling low imbalance loads, i.e., vibration caused by residual rotor imbalance. Basically, squeeze film dampers consist of an oil-filled annular cavity between two nonrotating surfaces, such as a bearing and a housing. When one surface moves relative to the other, the oil is squeezed and sheared, and generates hydrodynamic forces (References 1 and 2). These forces oppose the motion and reduce engine vibration response by dissipating energy in the form of heat.

Conventional dampers designed to control low and moderate imbalance loads are not effective under high imbalance loads. The high loads require large damper amplitudes, often larger than the damper clearance. This operating condition is highly nonlinear and leads to high load transmissibility caused by surface to surface contact and loss of damping due to oil leakage and film breakdown.

The damper concepts evaluated in this program can be designed to provide effective high and low load damping. This section contains a general description of each damper concept. The mathematical models used to analyze these damper systems are discussed in detail in Section 4.3.

3.2.1 Multi-Ring Damper

The multi-ring damper concept uses the capabilities of several squeeze films in series (see Figure 3.2-1). Two or more squeeze films are established by installing thin rings (which are neither centered nor externally supported) in the oil cavity. The cavity is either axially sealed or open. If the cavity is sealed, there is no axial flow in the damper; only circumferential flow is considered in the analysis. When the cavity is open, axial flow is assumed to predominate and circumferential flow is neglected.

Since the hydrodynamic forces in a squeeze film damper are inversely proportional to the third power of the clearance, a multi-ring damper has a significantly higher load carrying capacity at the same amplitude than a conventional squeeze film damper with the same total clearance. (Even though the series arrangement reduces effective stiffness and damping, the increase in dynamic forces resulting from the reduction in clearance exceeds the decrease due to the series arrangement.) As with conventional dampers, the forces produced by a multi-ring damper are nonlinear at high eccentricity ratios. However, proper design can reduce operating eccentricity ratios and provide effective high and low load damping capability.

Rotation and flotation of the intermediate rings make the multi-ring damper a difficult concept to analyze. But with certain basic assumptions (explained in detail in Section 4.3.1) high load damping capability can be effectively evaluated.

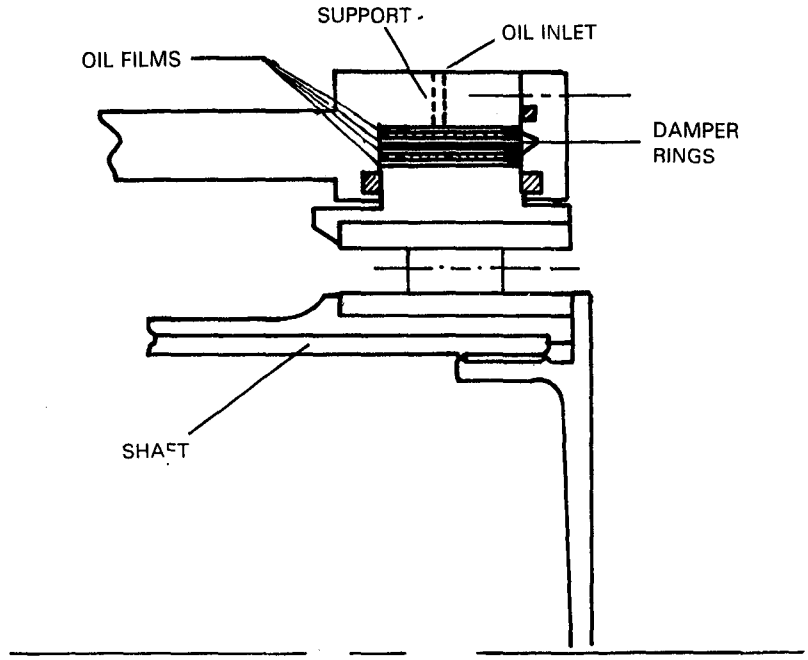

Figure 3.2-1 Multi-Ring Damper Concept

3.2.2 Cartridge Damper

A cartridge damper (see Figure 3.2-2) is a tightly sealed self-contained squeeze film damper filled with a highly viscous fluid. It can be either the short type (open to axial flow) or the long type (axially sealed).

The cartridge damper concept provides an attractive alternative to conventional squeeze film dampers. The high viscosity fluid used in the cartridge damper provides greater load carrying capacity than the bearing lubrication oil used in conventional dampers. In addition, the fluid can be pre-pressurized to suppress radial stiffness and increase damping forces. This control over fluid viscosity and supply pressure permits cartridge damper configurations to be tailored to the damping requirements for specific types of engines.

Because the cartridge damper is a sealed unit, an external system is required to extract the dissipated heat energy, thereby increasing complexity and weight. Further, since leakage can be critical, more periodic maintenance checks are required than with other damper concepts.

3.2.3 Curved Beam Damper

The curved beam damper (Figure 3.2-3) contains curved springs or beams which center the damper, provide radial stiffness, and maintain pockets of oil which are squeezed under load (Reference 3). Radial stiffness (which is related to beam flexibility) depends on the geometry of the beam and the boundary conditions at the end of the beam. Viscous damping capability is provided by pumping engine lubrication oil through inlet ports as the shaft whirls. In the analysis, it is assumed that the damping force is proportional to the fluid velocity, which is in turn proportional to the shaft whirl velocity.

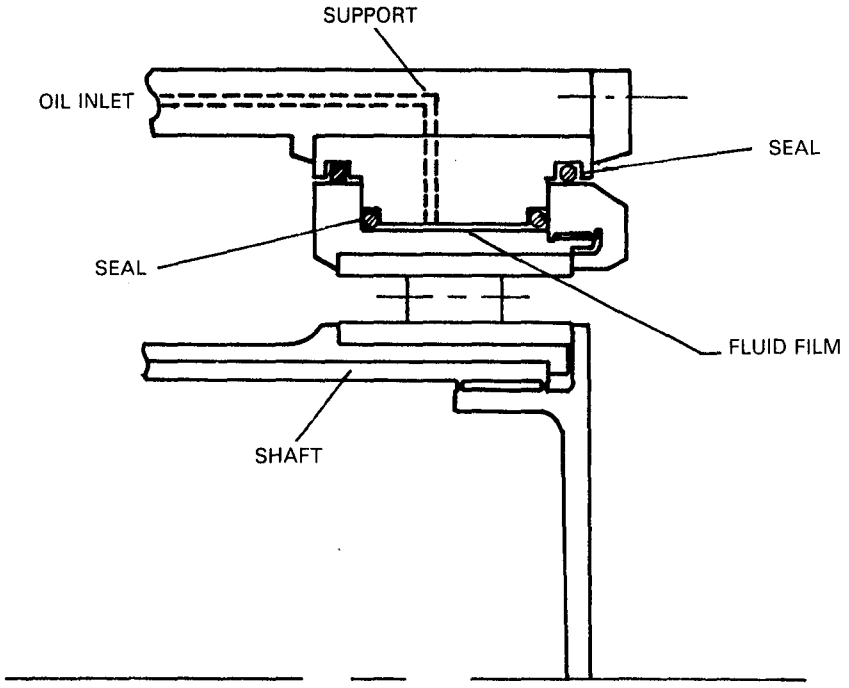

Figure 3.2-2 Cartridge Damper Concept

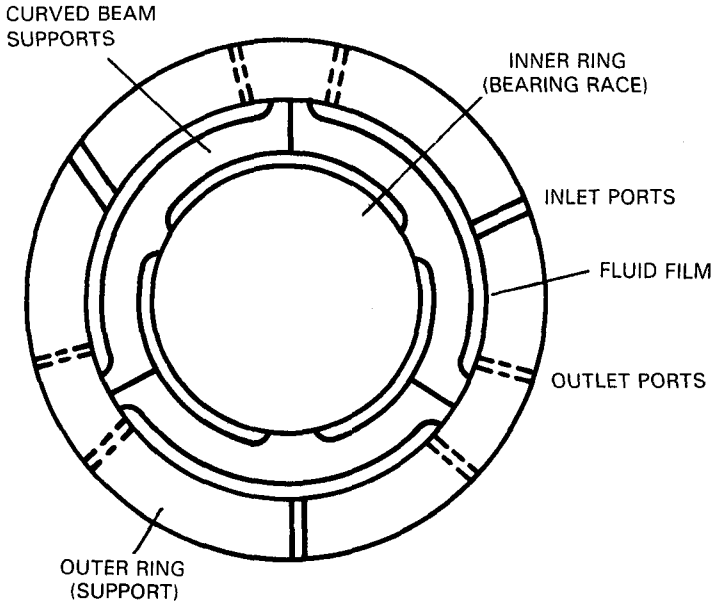

Figure 3.2-3 Curved Beam Damper Concept

The curved beam damper is compact, lightweight, and capable of handling larger imbalances than conventional squeeze film dampers. Properly-designed radial clearances and inlet and outlet ports will allow the damper to provide constant radial stiffness and damping coefficients over the entire operating range. It also has the advantage of independent control of stiffness and damping.

3.2.4 Viscous/Friction Damper

The viscous/friction damper consists of a number of annular friction plates, held together by an axial clamping force, operating in series with a conventional squeeze film damper (see Figure 3.2-4). This concept has been tested at Pratt & Whitney Aircraft to determine the damping characteristics of the friction plates (Reference 4). Effort is currently underway to investigate the combined viscous/friction damping characteristics.

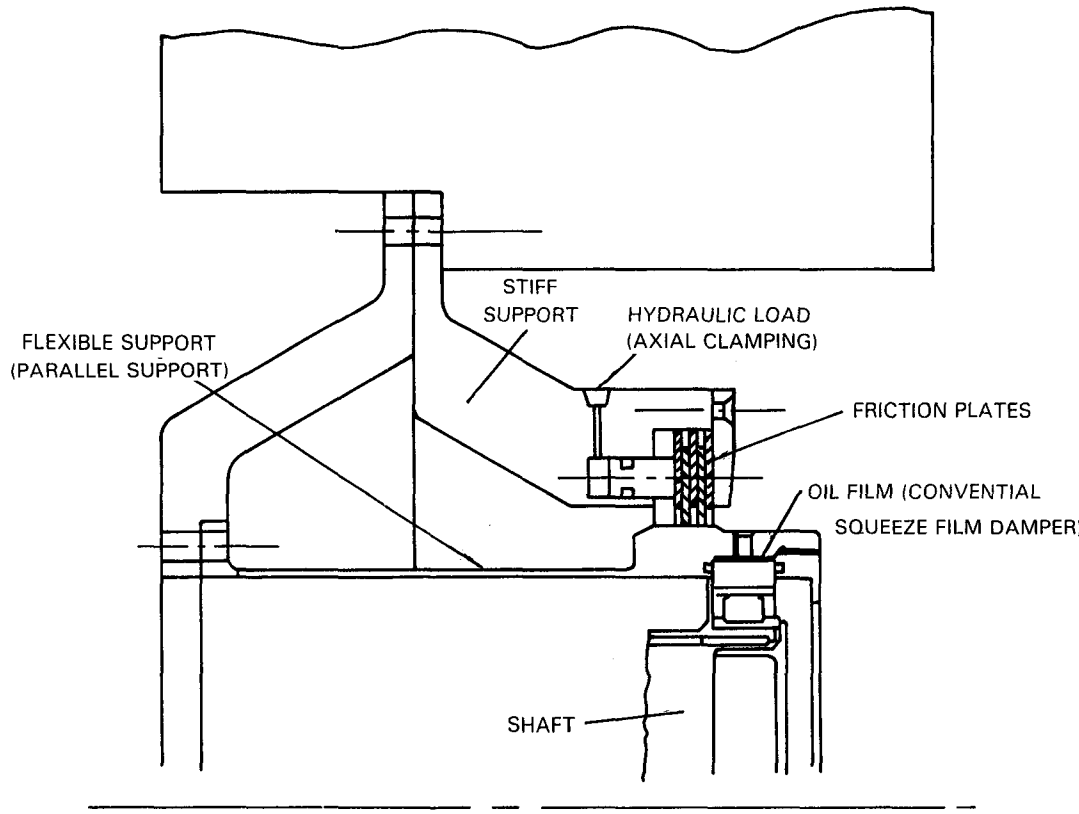

Figure 3.2-4 Viscous/Friction Damper Concept

In this system, the squeeze film damper controls residual rotor imbalance. However, when a specified load level is exceeded (e.g., following blade loss), the additional vibrational energy is dissipated by the friction plates. This dual damper concept provides a great deal of flexibility in designing a damper system which effectively satisfies both high and low load damping requirements. The viscous/friction damper is larger and heavier than the other damping systems, but the flexibility it provides can offset the weight penalty.

Because the friction plates are subject to wear, the viscous/friction damper will require periodic maintenance. Further, the friction force is constant at all damper amplitudes, making the system nonlinear over the operating range.

SECTION 4.0

ANALYTICAL METHODS.

4.1 CRITICAL SPEED ANALYSIS

A detailed analysis was conducted to identify the critical speeds for the representative large transport, military and general aviation engines. At these critical speeds, engine vibration response can exceed load and deflection limits, compromising engine performance and structural integrity. For many of the critical speed modes, vibration energy is absorbed by the engine case, bearings and supports, and additional damping is not required. However, with shaft bending modes, vibration energy cannot be completely controlled by the engine support structure, and additional damping is required. These modes are sensitive to imbalance and could be excited by foreign object damage or blade loss. In this study, a shaft bending mode was brought within the operating speed range of each engine. This mode was used to determine which type of high load damper would most effectively control vibration response in advanced jet engines.

Basically, a critical speed analysis provides detailed information on the natural frequency vibration modes which define the dynamic behavior of a jet engine. Gas turbines are multi-degree of freedom systems with distinct natural frequencies and corresponding mode shapes (ranging from vibration in the case to severe bending in the shaft). Due to gyroscopic effects and variable bearing properties, these natural frequencies depend on the operating speed of the engine. The speeds at which the natural frequency of the engine equals the rotational frequency are termed critical speeds. Operating the engine at these critical speeds without proper damping can affect engine performance and structural integrity.

For each critical speed, the mode shape and distribution of vibration energy throughout the engine are evaluated to determine the severity of the mode. If the mode is highly sensitive to external loads, such as blade loss and foreign object damage, it is desireable to drive the mode out of the operating speed range. If this approach is not feasible, engine vibration response can be analyzed under various conditions and a high load damping system developed. Engine vibration response depends on the magnitude and location of imbalance, operating speed, proximity of the critical speed, and damping capability already available in the engine.

Due to size and complexity, there is a variety of critical speed modes in a gas turbine engine. However, critical speed modes can be grouped in three general catgories:

1) Case Modes - Most of the activity or motion occurs in the case structure, where large amounts of strain energy and kinetic energy are generated. Because of material damping and friction at the flanges and bolt locations, case modes tend to be relatively insensitive to excitation by imbalance.

2) Rigid Body Modes - Rotors and/or cases deflect as rigid bodies. All of the strain energy in the system is distributed through the engine supports or the bearings and support structures connecting the rotor(s) and cases. (An entire rotor bouncing or pitching relative to the engine cases is considered a typical rigid body mode.) These modes may be sensitive to imbalance, but they can be controlled by conventional dampers.

3) Shaft Bending Modes - A significant degree of bending occurs in the rotor(s) where a considerable portion of the strain energy in the system is distributed. Synchronous shaft bending modes tend to be quite sensitive to imbalance; the shaft does not flex cyclically and hence does not dissipate energy through material damping or internal friction. More specifically, experience has shown that shaft bending modes with more than 25% of the total system strain energy in the shaft are so sensitive to imbalance that they must either be moved out of the operating range or controlled by a damping mechanism.

These categories provide a convenient framework for discussion; in practice, critical speed modes are quite complex and exhibit a combination of characteristics. In this study, emphasis was placed on shaft bending modes due to their sensitivity to imbalance and tendency to transmit high loads through the bearings and dampers.

The critical speed analysis used in this study is based on the Prohl approach (Reference 5). The steady state variables (deflection, slope, moment and shear) at lumped mass stations are defined by the transfer matrix method. Rotors, stators, and intermediate support structures are modeled as lines. Each line consists of a number of mass stations connected by massless spring elements. The mass stations account for inertia and gyroscopic effects while the spring elements represent bending and shear flexibilities. A beam bending approximation is used to calculate flexibilities between mass stations. Connections between two lines are defined by solving the shear force and moment equations at the joints. A characteristic determinant is obtained and a speed search is conducted to identify the critical speeds at which the determinant goes to zero. The critical speeds are then substituted back into the transfer matrix to generate the deflections, slopes, moments and shear forces at all the mass stations. The mode shape is defined by deflection and slope. Once this definition is complete, the percent distribution of kinetic energy and strain energy in each of the components is calculated.

Results of the analysis for each of the representative engines are presented on the following pages.

4.1.1 Large Transport Engine

Fifteen critical speed vibration modes were identified for the large transport engine. A high compressor vibration mode at 7783 rpm was selected for further analysis. This mode is characterized by a high level of strain energy in the high rotor (high pressure compressor and turbine) which is difficult to dissipate without an external damping mechanism. In addition, there is a great deal of motion at the compressor, indicating a sensitivity to compressor imbalance. An advanced large transport engine is expected to operate safely at this speed under high levels of imbalance. Installing a high load damper at the Number 2 bearing provides a method of satisfying this requirement.

The representative large transport engine is a dual rotor turbofan. The low rotor, which is supported on two antifriction bearings, runs between 1000 rpm and 3800 rpm. The high rotor, which is also supported on two antifriction bearings, operates between 4700 rpm and 8500 rpm. Separate critical speed analyses were conducted to obtain low rotor excited critical speeds and high rotor excited critical speeds. Gyroscopic effects were evaluated by assuming a linear speed relation between the two rotors. Results of the analyses are summarized in Figures 4.1-1 and 4.1-2. For simplicity, only the synchronous rotor mode shape is presented in the figures and the percent distribution of energy in the other components is listed. The distribution indicates the degree of participation of other rotor and static (nonrotating) structures. A more detailed discussion of the analyses follows.

4.1.1.1 Low Rotor Excited Modes

The low rotor excited modes shown in Figure 4.1-1 tend to be relatively insensitive to low rotor imbalance. Significant amounts of vibration energy are dissipated in the case structure or high rotor.

The first and third modes at 748 and 2243 rpm are classic case modes. Over 90% of the system activity, as measured by kinetic and strain energy levels, is found in the case structure. These modes benefit from material and coulomb damping in the cases and are very insensitive to imbalance.

The remaining modes at 1388, 2808 and 3452 rpm show increased low rotor activity, but they are still predominantly case modes with over 65% of the system strain energy in cases and supports. These modes also show some coupling with high rotor modes, as evidenced by the increased strain energy in cases and supports. However, this high rotor activity is of little concern; experience has shown that these coupled modes are not easily excited from the low rotor through the case to the high rotor. The fifth mode at 3452 rpm has the highest level of low rotor activity and the greatest sensitivity to low rotor imbalance. This mode is not considered sensitive enough to require control via squeeze film dampers or any other damping mechanism.

LOW ROTOR CRITICAL SPEEDS

BELOW IDLE

SPEED	MODE SHAPE (LOW ROTOR)	ENERGY DISTRIBUTION		
		LOW ROTOR	HIGH ROTOR	CASE STRUCTURE
748	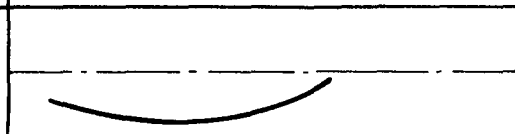	KINETIC ENERGY = 4% STRAIN ENERGY = 1% BEARING NO. 1 = 0% BEARING NO. 4 = 0%	4% 0% NO. 2 0% NO. 3 0%	92% 99%

ABOVE IDLE

SPEED	MODE SHAPE (LOW ROTOR)	ENERGY DISTRIBUTION		
		LOW ROTOR	HIGH ROTOR	CASE STRUCTURE
1388	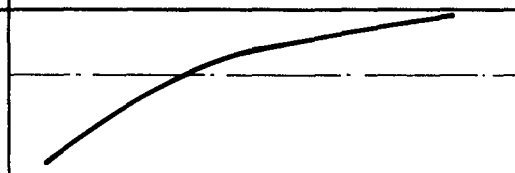	KINETIC ENERGY = 21% STRAIN ENERGY = 2% BEARING NO. 1 = 0% BEARING NO. 4 = 1%	17% 1% NO.2 0% NO. 3 1%	62% 95%
2243		KINETIC ENERGY = 8% STRAIN ENERGY = 5% BEARING NO. 1 = 0% BEARING NO. 4 = 1%	2% 0% NO. 2 1% NO. 3 1%	90% 92%
2808		KINETIC ENERGY = 7% STRAIN ENERGY = 1% BEARING NO. 1 = 1% BEARING NO. 4 = 1%	30% 1% NO. 2 0% NO. 3 7%	63% 89%
3452		KINETIC ENERGY = 46% STRAIN ENERGY = 14% BEARING NO. 1 = 7% BEARING NO. 4 = 4%	21% 1% NO. 2 0% NO. 3 7%	33% 67%

Figure 4.1-1 Low Rotor Critical Speed Mode Shapes and Energy Distribution; Large Transport Engine

HIGH ROTOR CRITICAL SPEEDS

BELOW IDLE

SPEED	MODE SHAPE (LOW ROTOR)	ENERGY DISTRIBUTION		
		HIGH ROTOR	LOW ROTOR	CASE STRUCTURE
1334	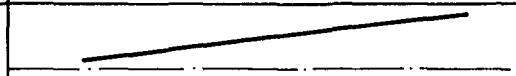	KINETIC ENERGY = 18% STRAIN ENERGY = 1% BEARING NO. 2 = 0% BEARING NO. 3 = 1%	28% 8% NO. 1 0% NO. 4 1%	54% 89%
1963		KINETIC ENERGY = 5% STRAIN ENERGY = 1% BEARING NO. 2 = 0% BEARING NO. 3 = 1%	72% 77% NO. 1 1% NO. 4 2%	25% 18%
2161	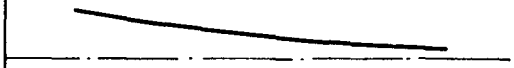	KINETIC ENERGY = 2% STRAIN ENERGY = 1% BEARING NO. 2 = 0% BEARING NO. 3 = 0%	20% 11% NO. 1 0% NO. 4 1%	78% 86%
2746	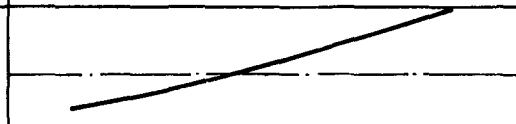	KINETIC ENERGY = 35% STRAIN ENERGY = 2% BEARING NO. 2 = 0% BEARING NO. 3 = 8%	4% 2% NO. 1 0% NO. 4 1%	61% 87%
3512	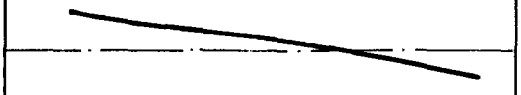	KINETIC ENERGY = 7% STRAIN ENERGY = 1% BEARING NO. 2 = 1% BEARING NO. 3 = 2%	44% 22% NO. 1 0% NO. 4 2%	49% 72%
3755	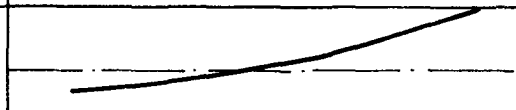	KINETIC ENERGY = 16% STRAIN ENERGY = 2% BEARING NO. 2 = 0% BEARING NO. 3 = 7%	33% 12% NO. 1 1% NO. 4 5%	51% 73%

Figure 4.1-2 High Rotor Critical Speed Mode Shapes and Energy Distribution; Large Transport Engine

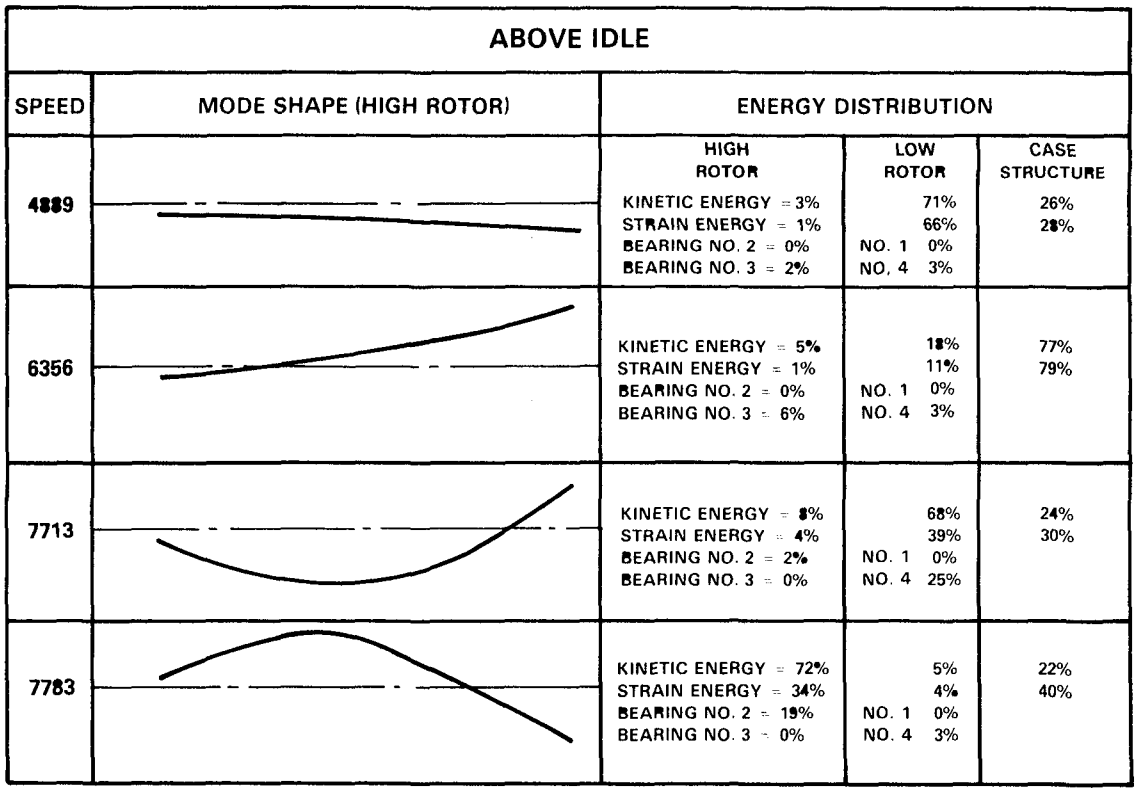

Figure 4.1-2 Continued

4.1.1.2 High Rotor Excited Modes

In general, the high rotor excited modes shown in Figure 4.1-2 show more coupling between the low rotor, high rotor, and cases than the low rotor excited modes. Further, the distribution of strain energy and kinetic energy for the tenth mode (7783 rpm) was of enough concern to warrant high load damping at the Number 2 bearing.

There are several high rotor excited case modes which are of little concern. Specifically, these are the first, third, fourth, and eighth modes at 1334, 2161, 2746 and 6356 rpm respectively. The first, third and eighth modes have small amounts of low rotor participation, but the major strain energy is distributed in the case, indicating that they are insensitive to high rotor imbalance. The fourth mode is a case mode coupled with a rigid body high rotor mode. This mode has a greater sensitivity to high rotor imbalance than the other three, but the level of sensitivity is not great enough to require a damping system.

The second, seventh and ninth modes at 1963, 4889 and 7713 rpm respectively show substantial strain and kinetic energy in the low rotor and are therefore labeled high rotor excited low rotor modes. As with low rotor excited high rotor modes, these modes are not easily excited from the high rotor through the case to the low rotor.

The fifth and sixth modes at 3512 and 3755 rpm are high rotor excited modes, coupled with both the low rotor and the cases, with slightly more strain and kinetic energy in the cases. These modes would benefit from the material and coulomb damping in the cases and tend to be insensitive to imbalance.

The tenth mode at 7783 rpm will be used in evaluating high load damping requirements for a large transport engine. This mode is within the speed range where an advanced engine would be expected to operate safely under high levels of imbalance. The high level of strain energy in the rotor is difficult to dissipate without an external damping mechanism. The high level of kinetic energy indicates significant sensitivity to compressor imbalance. The large amount of strain energy in the Number 2 bearing points to large displacements at that location. An external damping mechanism can dissipate the energy which would be generated under forced vibrations. A high load damper at the Number 2 bearing location will effectively control this mode under compressor blade loss.

4.1.2 Small General Aviation Engine

Six critical speed vibration modes were identified for the small general aviation engine. A turbine vibration mode at 9355 rpm was selected for further analysis. This mode is characterized by high levels of strain and kinetic energy in the rotors and significant sensitivity to turbine imbalance. A high load damper at the Number 3 bearing should control engine vibration response under imbalance conditions.

The representative small general aviation engine is a single rotor turbojet. The rotor comprises the compressor and turbine. It is supported on three bearings and has a rotor speed range of 9000 to 20,000 rpm. Results from the critical speed analysis are summarized in Figure 4.1-3. Again, to simplify interpretation, only the rotor mode shape is shown in the figure, but the percent distribution of energy in both the rotor and case structure is listed.

Of the six modes in the speed range, four were considered to be of little concern in this study. The second mode at 2236 rpm is a classic case mode with over 95% of the total system strain and kinetic energy in the case structure. The first, third, and sixth modes at 1406, 4176 and 16,261 rpm respectively also have substantial activity in the case structure (over 75% of the total strain energy), but these modes also have some degree of rotor participation (indicated by the rotor kinetic energy levels of over 35%). However, these modes tend to be insensitive to imbalance due to effective material and coulomb damping in the case.

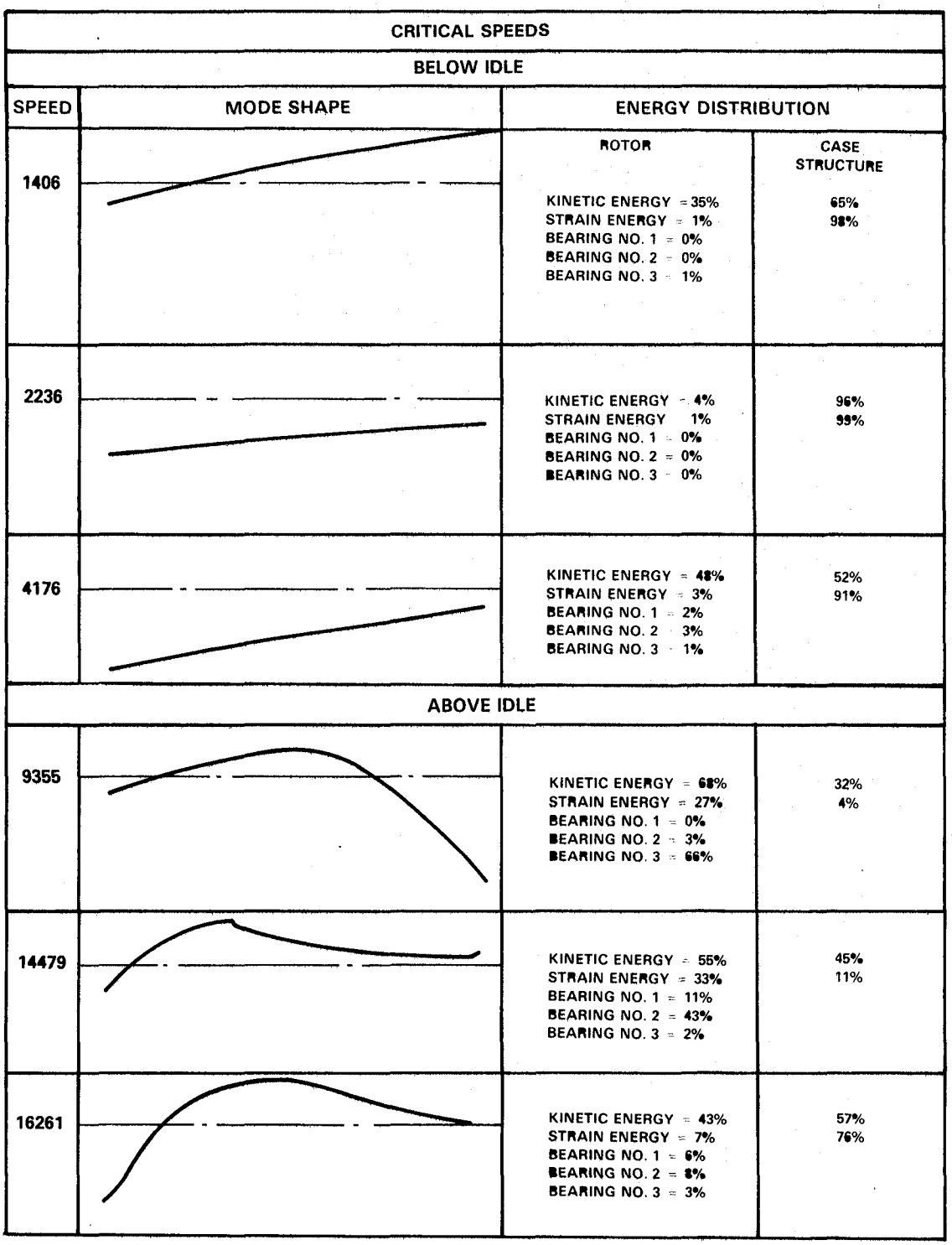

Figure 4.1-3 Critical Speed Mode Shapes and Energy Distribution; Small General Aviation Engine

The fourth and fifth modes (9355 and 14,476 rpm) show high levels of strain and kinetic energy in the rotors. These results point up a sensitivity to imbalance which would require an external damping mechanism at the bearings. For the fourth mode, most of the rotor motion is directed back toward the turbine. This mode would therefore be most sensitive to turbine imbalance, but it could be controlled by a damper at the Number 3 bearing. The fifth mode has large rotor amplitudes in the compressor section and would therefore be sensitive to compressor imbalance. A damper at the Number 2 bearing would effectively control this mode. Study of either mode would provide insight into the high load damping requirements for this engine. However, the turbine mode was selected because experience has shown that turbine operating temperatures and material limitations make it susceptible to blade loss. In addition, the load on the Number 3 bearing for the turbine mode is higher than the load on the Number 2 bearing for the compressor as shown by the amount of strain energy in the Number 3 bearing.

4.1.3 Military Engine

Thirteen critical speed vibration modes were identified for the military engine. A low turbine vibration mode at 7164 rpm was selected for further analysis. This mode is characterized by a high level of strain energy in the low rotor and a sensitivity to turbine imbalance which would be difficult to control under high loads. Installing a damper at the Number 5 bearing appears to be the most effective method of controlling this mode.

The representative military engine is a two rotor turbofan with an augmentor. The low rotor, which includes the three stage fan and low pressure turbine, is supported on three antifriction bearings and operates between 4700 rpm and 11,500 rpm. The high speed rotor, which includes the high pressure compressor and high pressure turbine, is supported on two antifriction bearings and operates between 8000 rpm and 14,700 rpm. As with the large transport engine, separate critical speed analyses were conducted to obtain low and high rotor excited critical speed modes. Similarily, gyroscopic effects were evaluated by assuming a linear speed relationship between the rotors. The results of the analyses are summarized in Figures 4.1-4 and 4.1-5. The summary shows the critical speeds, synchronous rotor mode shapes and energy distribution among all the major components. A more detailed discussion of the analyses follows.

4.1.3.1 Low Rotor Excited Modes

Five low rotor excited modes were identified for the military engine. Each of the modes has a large amount of energy in the case structure, but the fifth mode at 7164 rpm showed a siginificant degree of low rotor bending, indicating that a high load damper is required at the Number 5 bearing.

The first three modes at 1360, 2131 and 3307 rpm respectively have an appreciable amount of case participation with over 90% of the system strain energy and over 55% of the system kinetic energy in the case and mount structure. The second and third modes are case modes coupled with high and low rotor modes respectively, but strain energy levels in the low rotor do not indicate sensitivity to low rotor imbalance. Further, the high levels of strain energy in the case structures indicate the presence of sufficient material and coulomb damping to control the modes.

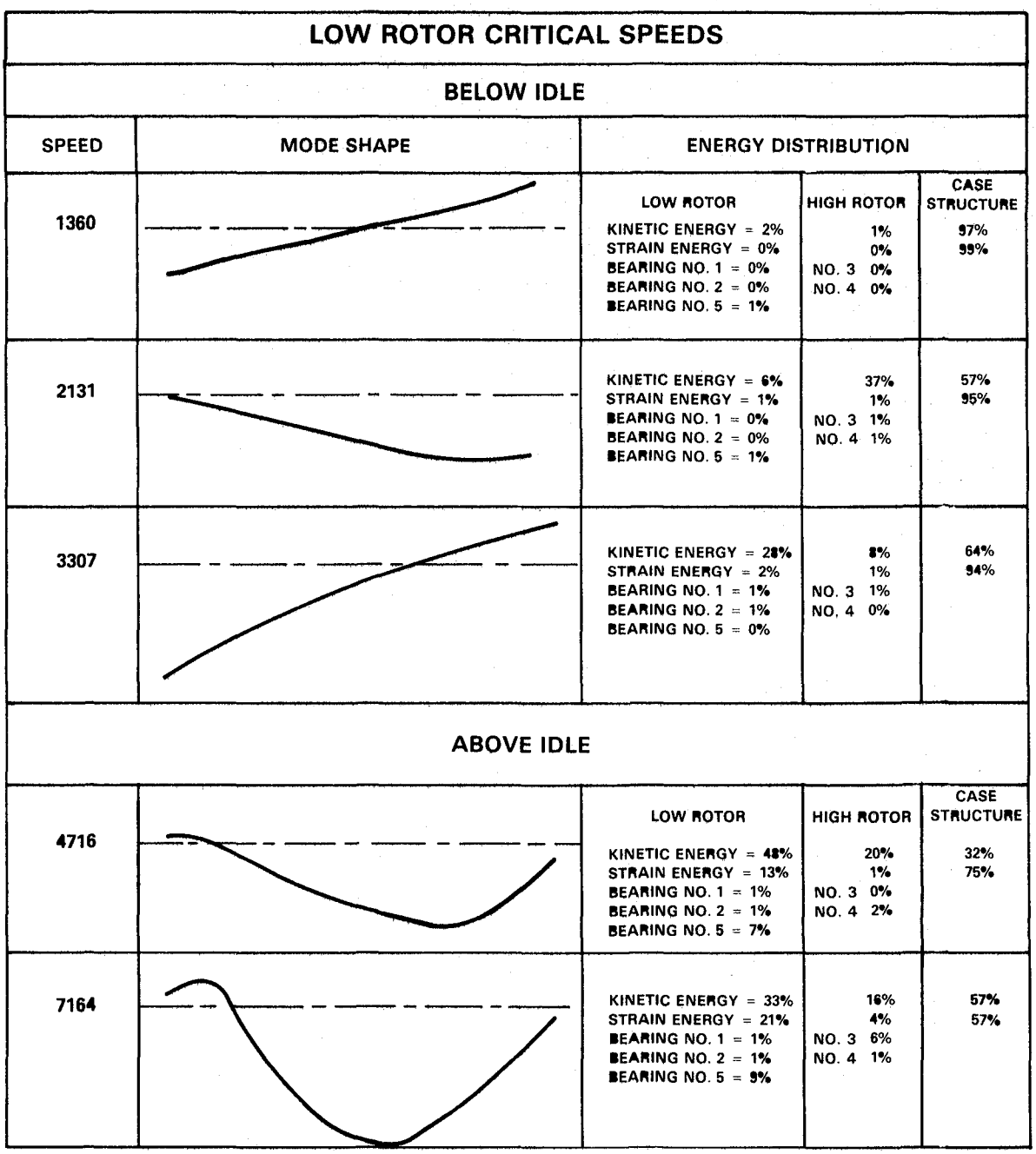

Figure 4.1-4 Low Rotor Critical Speed Mode Shapes and Energy Distribution; Military Engine

The fourth and fifth modes at 4716 and 7164 rpm have more significant levels of strain energy and kinetic energy in the low rotor and could be sensitive to imbalance. The fifth mode has greater strain energy in the low rotor, indicating somewhat higher sensitivity to imbalance, while lower strain energy in the cases indicates less material and coulomb damping than the fourth mode. The fifth mode is therefore of greater interest in evaluating high load damping requirements. In addition, experience has shown that this mode is sensitive to low turbine blade loss imbalance and may be difficult to control under high loads. The Number 5 bearing location has the highest low rotor bearing load and would therefore be the appropriate location for a damper.

HIGH ROTOR CRITICAL SPEEDS

BELOW IDLE

SPEED	MODE SHAPE	ENERGY DISTRIBUTION		
		HIGH ROTOR	LOW ROTOR	CASE STRUCTURE
2253	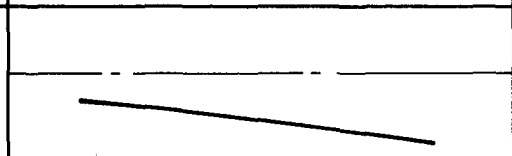	KINETIC ENERGY = 38% STRAIN ENERGY = 1% BEARING NO. 3 = 0% BEARING NO. 4 = 1%	12% 1% NO. 1 2% NO. 2 0% NO. 5 14%	50% 81%
3221	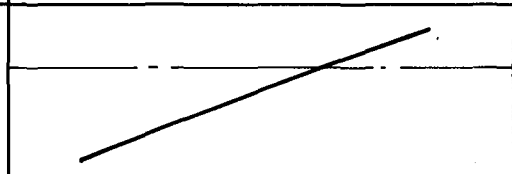	KINETIC ENERGY = 9% STRAIN ENERGY = 1% BEARING NO. 3 = 1% BEARING NO. 4 = 0%	NO. 1 37% NO. 2 7% NO. 5 4% 2% 1%	54% 84%
5515	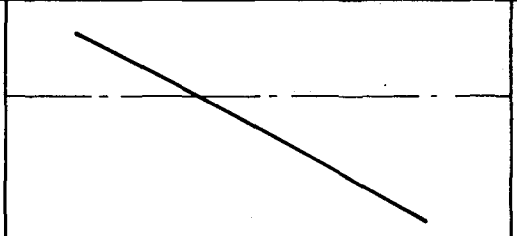	KINETIC ENERGY = 20% STRAIN ENERGY = 4% BEARING NO. 3 = 1% BEARING NO. 4 = 2%	NO. 1 13% NO. 2 2% NO. 5 4% 1% 2%	67% 84%
5823	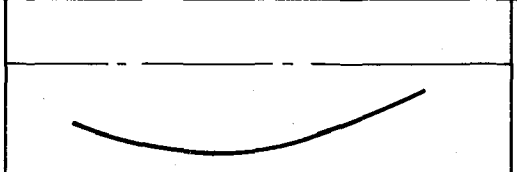	KINETIC ENERGY = 15% STRAIN ENERGY = 3% BEARING NO. 3 = 4% BEARING NO. 4 = 1%	NO. 1 38% NO. 2 21% NO. 5 21% 1% 0%	47% 49%
7404	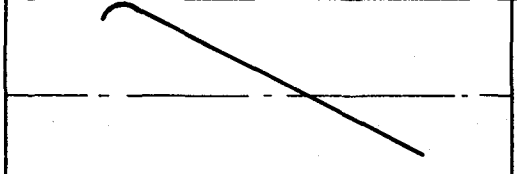	KINETIC ENERGY = 41% STRAIN ENERGY = 15% BEARING NO. 3 = 18% BEARING NO. 4 = 1%	3% 1% NO. 1 5% NO. 2 1% NO. 5 0%	56% 59%
8455	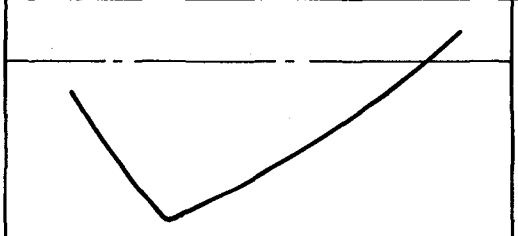	KINETIC ENERGY = 44% STRAIN ENERGY = 20% BEARING NO. 3 = 28% BEARING NO. 4 = 1%	3% 2% NO. 1 0% NO. 2 1% NO. 5 0%	53% 48%

Figure 4.1-5 High Rotor Critical Speed Mode Shapes and Energy Distribution; Military Engine

ABOVE IDLE				
SPEED	MODE SHAPE	ENERGY DISTRIBUTION		
		HIGH ROTOR	LOW ROTOR	CASE STRUCTURE
10091	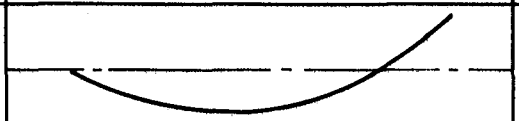	KINETIC ENERGY = 3% STRAIN ENERGY = 2% BEARING NO. 3 = 1% BEARING NO. 4 = 1%	8% 4% NO. 1 1% NO. 2 2% NO. 5 1%	89% 88%
13615		KINETIC ENERGY = 2% STRAIN ENERGY = 3% BEARING NO. 3 = 1% BEARING NO. 4 = 1%	47% 43% NO. 1 1% NO. 2 10% NO. 5 1%	51% 40%

Figure 4.1-5 Continued

4.1.3.2 High Rotor Excited Modes

Eight high rotor excited modes were identified for the military engine. These modes have various amounts of low rotor, high rotor, and case participation, but none was considered significant enough to warrant further analysis.

The first, third and seventh modes at 2253, 5515 and 10,091 rpm respectively are primarily case modes, with over 50% of the total kinetic energy and over 80% of the total strain energy in the case structure. The first and third modes have some rigid body motion of the high rotor, but none of these modes has sufficient rotor strain energy to be sensitive to high rotor imbalance.

The second, fourth and eighth modes at 3221, 5823 and 13,615 rpm respectively are high rotor excited low rotor modes with 35% to 50% of the total kinetic energy in the low rotor and 40% to 80% of the total strain energy in the cases. These modes would be insensitive to high rotor imbalance due to available damping in the case structure and the minimum participation of the high rotor in the energy distribution.

The fifth and sixth modes at 7404 and 8455 rpm have significant high rotor participation, with over 15% of the strain energy and over 40% of the kinetic energy in the high rotor. These modes are similar to the high compressor (tenth) mode which was selected for study in the large transport engine, and they also tend to be sensitive to high compressor imbalance. Both modes can be controlled by a damper at the Number 3 bearing because of the displacement and load at this location. Either of these modes could have been selected for analysis, but the results would be similar to the large turbofan study. An evaluation of damping requirements for the low turbine vibration mode was considered to be of greater value in this study.

4.2 FORCED RESPONSE ANALYSIS

Even though the critical speeds of an engine indicate possible regions of concern, they may not necessarily impede the safe operation of an engine. Engine response which affects performance and safety is dependent on the type, magnitude and location of applied forces, the availability of damping and nonlinearity among the various structural elements. Only a complete forced vibration analysis can provide a thorough understanding of the engine under different external loads (inherent imbalance, blade loss, bowed rotor etc.)

Pratt & Whitney Aircraft has developed a sophisticated steady-state forced-response analysis to predict engine response under various dynamic loads (Reference 6). It is based on the standard transfer matrix method but can efficiently account for nonlinear springs, nonlinear viscous dampers, coulomb dampers etc. This multishaft analysis is a widely-used design tool at different stages of engine development. For a given set of forces, this analysis generates deflections, slopes, moments and shear forces at different locations over the entire speed range. The relative motion between the rotor and the case, dynamic loads through the support structures, and absolute deflections of critical case structure locations are evaluated to assure efficient and safe operation of the engine.

In this program, forced response analysis has been used to determine damper requirements and to evaluate engine performance with the damper concepts which were selected. The results of the efforts to determine damper requirements are discussed below.

4.2.1 Large Transport Engine

As discussed in Section 4.1.1, the high compressor mode of 7783 rpm was considered to be the most troublesome and has been selected for high load damper evaluation. The non-dimensionalized mode shape is shown in Figure 4.2-1. Due to its location and weight, first stage blade loss can generate large imbalance forces on the rotor and engine safety can be impaired. The first stage is also susceptible to foreign object damage.

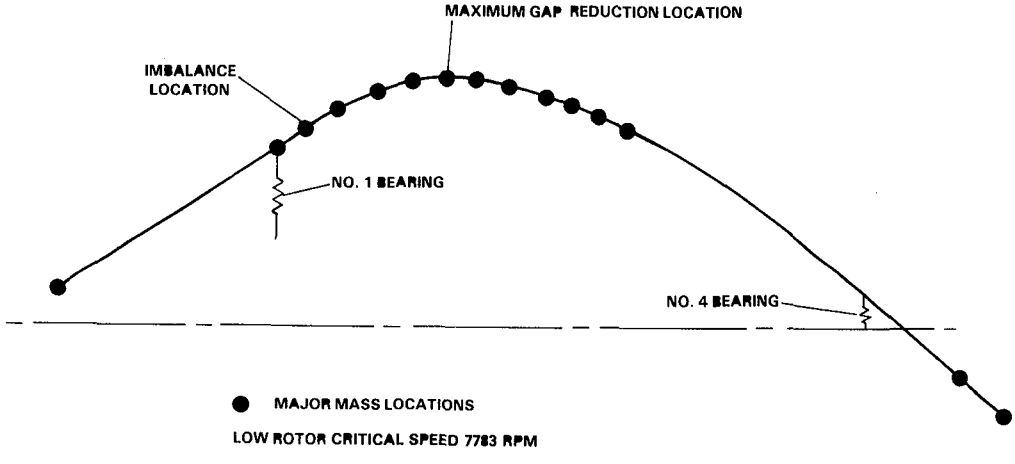

Figure 4.2-1 Critical Mode Shape (Rotor Only); Imbalance Location and Critical Deflection Location; Large Transport Engine

Although engine response at many locations should be evaluated to ascertain the safety margin, many times only one or two locations are studied for preliminary design. The responses at those location(s) are considered to represent the overall engine response under specific load conditions. It is assumed that if these responses meet the design limits, then the total engine also meets the design limits.

In the large transport engine, the high pressure compressor mode was judged to be the mode of concern, since it can be excited by compressor blade loss. The critical speed mode shape showed that deflection of the compressor and the support load at the Number 2 bearing would be high enough to be critical for safe operation of the engine. Therefore, engine response requirements were defined in terms of high pressure compressor deflection and Number 2 bearing support load. Details of these requirements are discussed in Section 5.1.1.

As a preliminary step toward selection of a proper damper (at the Number 2 bearing location), a parametric study on forced response analysis was completed. The fifth stage compressor gap closure and Number 2 support load sensitivities were obtained for various values of support stiffness and support damping. Seventy-two gm-cm, one oz-in., imbalance was used at the first-stage and the speed range of 6200 to 9200 rpm was searched for a peak response. It is assumed here that the engine response is linear and that the response for any imbalance is directly proportional to the response for 1 oz-in., 72 gm-cm. Stiffness up to 350 MN/m (2 x 10^6 lb/in) and damping up to 53000 N-S/m (300 lb sec/in) were considered. Any higher values pushed the peak response speed outside the selected speed range. Although the response within the operating range could be controlled by such a shift, applying such high stiffness and damping was considered an unacceptable solution. Besides, maintaining the peak response speed within the operating range guaranteed an effective evaluation of the high load damper concepts. Hence, only those values of stiffness and damping where the peak response speed was between 6200 rpm and 9200 rpm were considered.

The results are shown in Figures 4.2-2 and 4.2-3. Figure 4.2-2 illustrates the maximum gap reduction at the compressor while the maximum support load is shown in Figure 4.2-3. The corresponding support deflection which is necessary for a damper design is shown in Figure 4.2-4.

The large transport engine showed a low sensitivity to imbalance. As expected, higher damping and lower stiffness improved engine response. It was also interesting to note that at low stiffness 18 MN/m (1 x 10^5 lb/in), an increase in damping did not affect the responses.

By knowing the deflection and load requirements at high imbalance, the response sensitivities (deflections/unit imbalance, load/unit imbalance) can be determined. Assuming a linear engine response, the desired stiffness and damping can be determined from these graphs. A concept can then be designed to generate this desired stiffness and damping at the excursions given by the graph in Figure 4.2-4.

The damper requirements selected to meet the high load imbalance requirement in a large transport engine are discussed in Section 5.2.1.

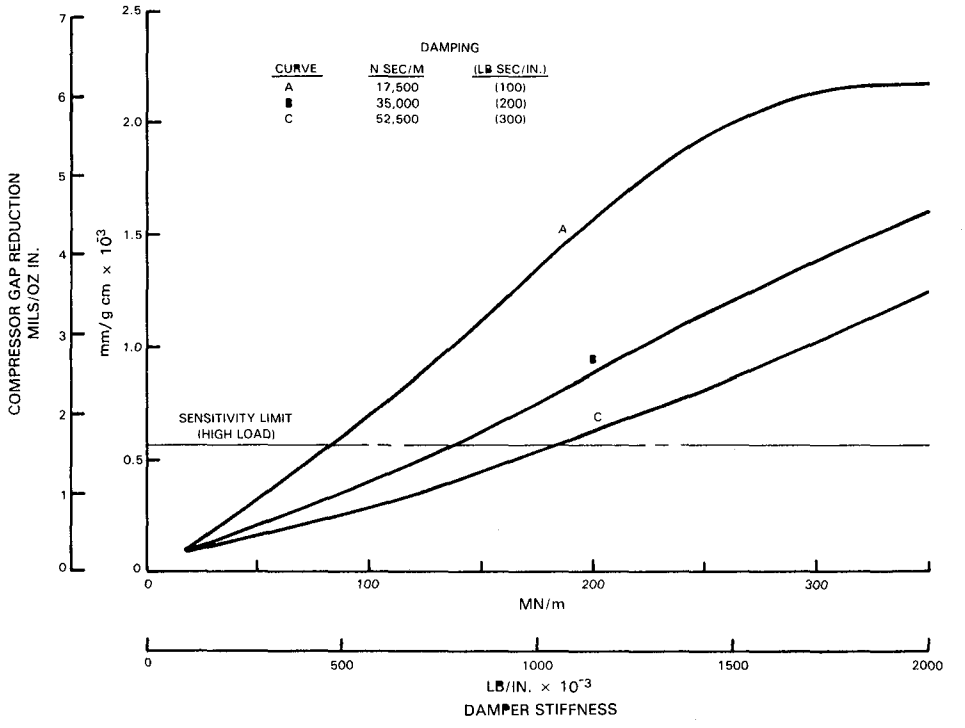

Figure 4.2-2 Fifth Stage Compressor Gap Reduction Sensitivity; Large Transport Engine

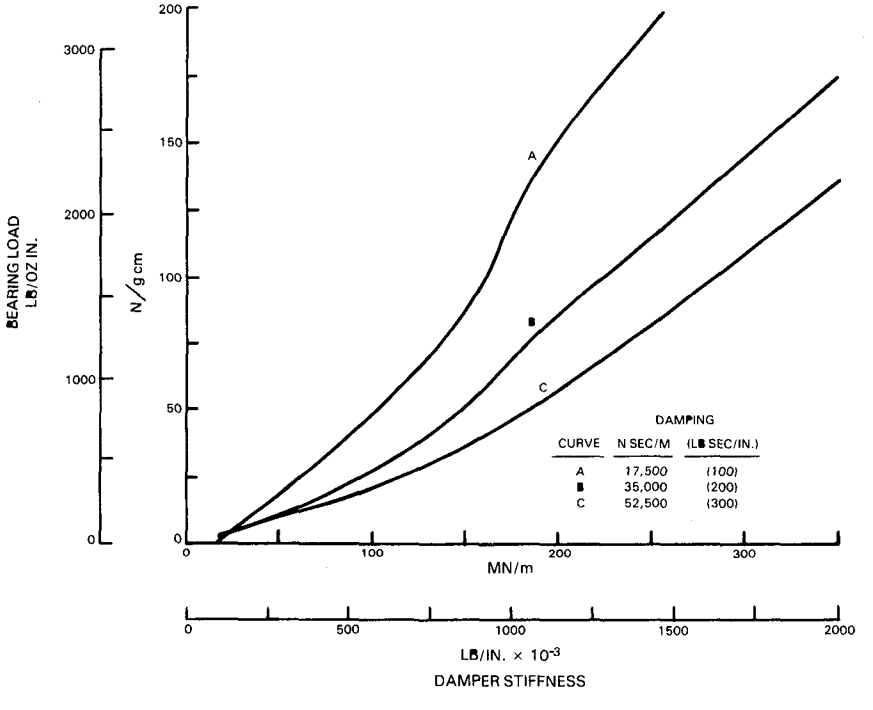

Figure 4.2-3 Number 2 Bearing Support Load Sensitivity; Large Transport Engine

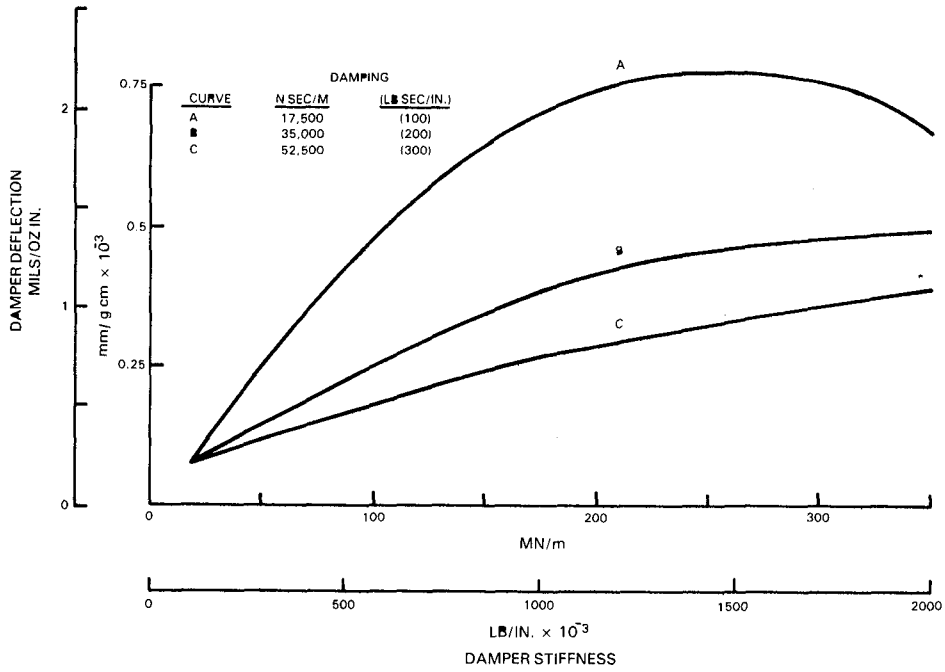

Figure 4.2-4 Support Deflection Response Sensitivities; Large Transport Engine

4.2.2 Small General Aviation Engine

In the representative small general aviation engine, the turbine mode at 9355 rpm has been chosen for high load damper evaluation (Section 4.1.2). The nondimensionalized mode shape is shown in Figure 4.2-5. It is sensitive to turbine imbalance and first or second stage turbine blade loss can seriously affect engine integrity. The gap closure at the second turbine stage and support load at the Number 3 bearing were judged to represent the most severe engine response under imbalance. Criteria to meet the safety margins were set on those responses and are discussed in Section 5.1.2.

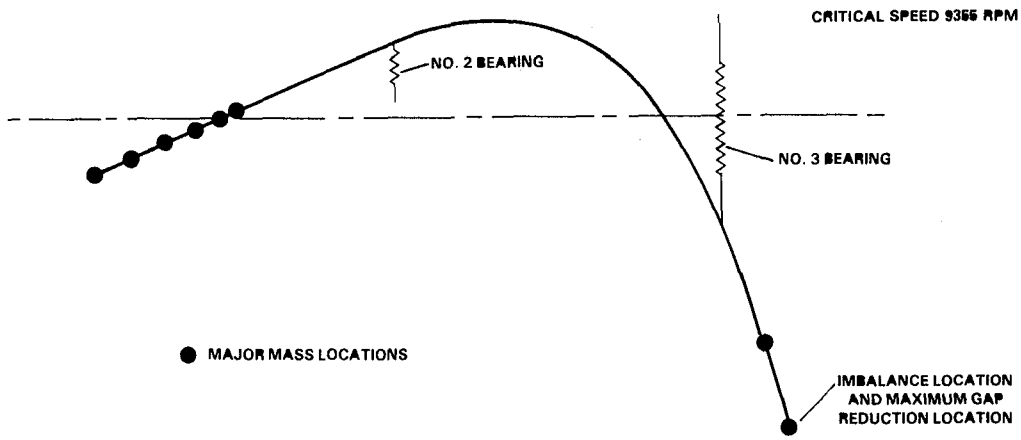

Figure 4.2-5 Critical Mode Shape (Rotor Only); Imbalance Location and Critical Deflection Location; Small General Aviation Engine

A parametric study was completed to determine response sensitivities by varying support stiffness and support damping. The peak response speed was maintained between 8000 rpm and 12,000 rpm. The peak responses for 72 gm-cm (1 oz-in) of unbalance are shown in Figures 4.2-6 and 4.2-7. The corresponding support motion is presented in Figure 4.2-8. Although the increase in damping improved the gap closure sensitivity, no significant reduction was achieved above 17500 N-S/m (100 lb sec/in.) As expected, the gap closure increased as support stiffness was increased. But the support loads at a stiffness lower than 26 MN/m (1.5 x 10^5 lb/in) showed an unexpected trend when damping was changed from 17500 to 26300 N-S/m (100 to 150 lb sec/in.) This could be due to the nonlinear dependence of the support load on support stiffness and damping.

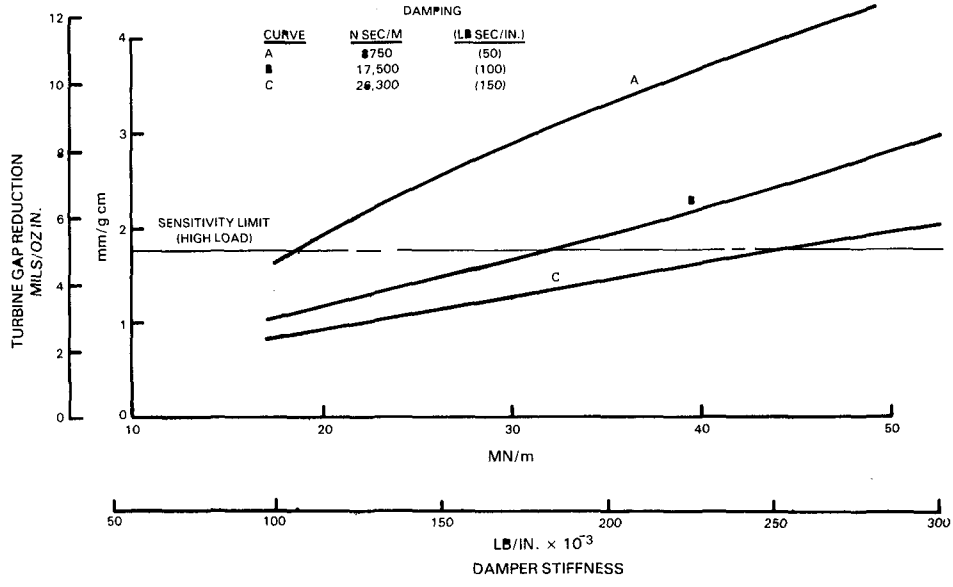

Figure 4.2-6 Second Stage Turbine Gap Reduction Sensitivity; Small General Aviation Engine

From Figures 4.2-6 and 4.2-7 and desired sensitivities, a suitable combination of support stiffness and damping can be selected to assure safe operation of the engine under turbine blade loss. A damper concept applicable to this engine can then be designed to provide that combination of stiffness and damping at the amplitudes shown in Figure 4.2-8.

The selected combination of damper parameters to meet the requirements in a small general aviation engine is discussed in Section 5.2.2.

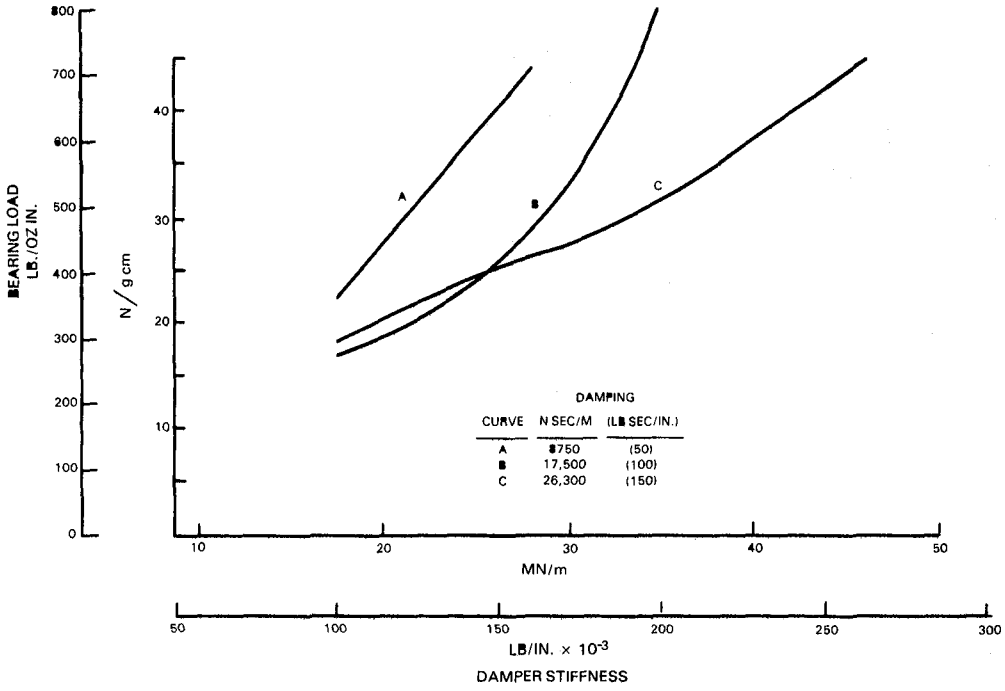

Figure 4.2-7 Number 3 Bearing Support Load Sensitivity; Small General Aviation Engine

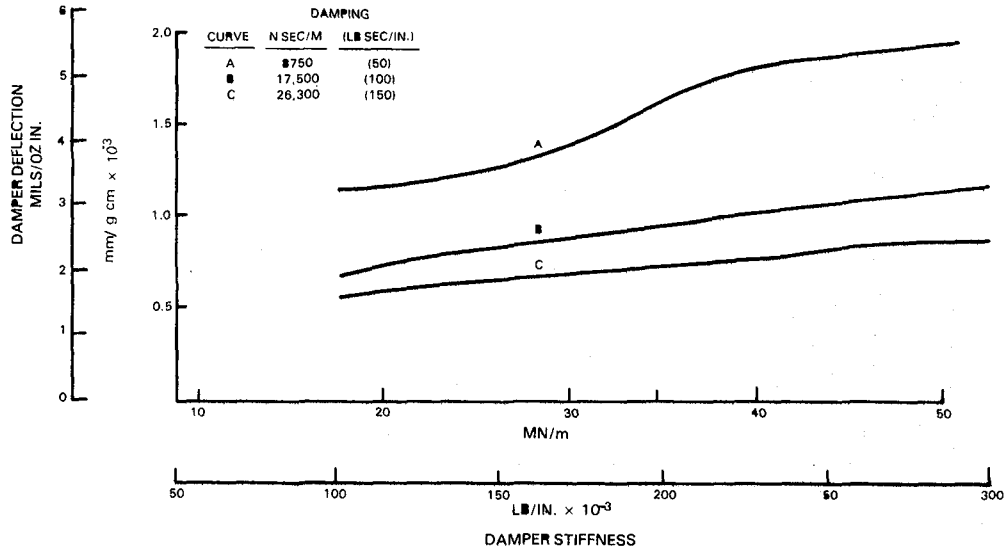

Figure 4.2-8 Support Deflection Response Sensitivities; Small General Aviation Engine

4.2.3 Military Engine

The representative military engine has a low turbine mode which is sensitive to imbalance within the operating range. The nondimensionalized mode shape is shown in Figure 4.2-9. Blade loss at the first or second stage turbine generates high imbalance forces which can result in high rotor deflections and large support loads. The gap reduction at the first turbine stage and the load on the Number 5 bearing support were considered to be representative of the overall response of the engine under turbine imbalance. The safety limits which were defined in terms of these responses are presented in Section 5.1.3.

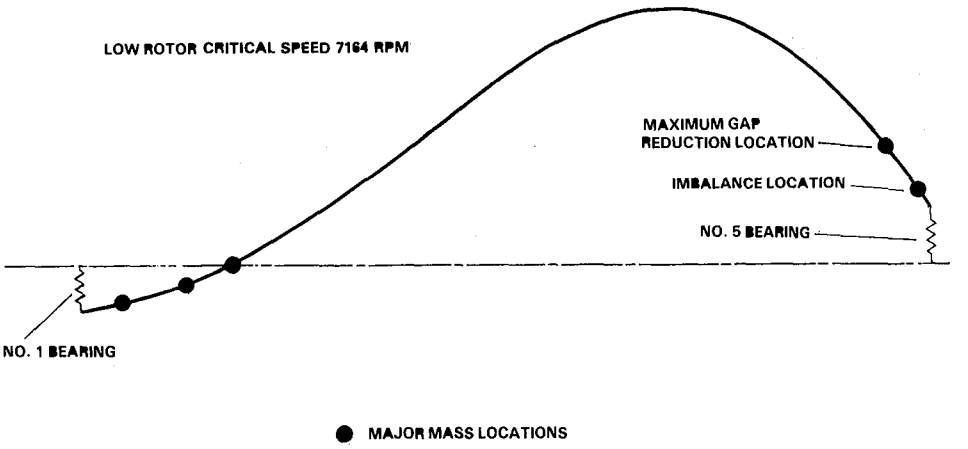

Figure 4.2-9 Critical Mode Shape (Rotor Only); Imbalance Location and Critical Deflection Location; Military Engine

A parametric study was conducted to obtain the sensitivity of turbine gap reduction and support due to second stage imbalance. The stiffness and damping coefficients at the Number 5 bearing location were varied and the speed range from 5500 to 8500 rpm was searched for peak responses. The results are shown in Figures 4.2-10 and 4.2-11. The corresponding rotor deflection at the support is shown in Figure 4.2-12. The gap closure and support load were sensitive to support stiffness but were relatively insensitive to support damping. At low support stiffness, higher damping actually increased the gap closure indicating the existence of optimum damping. Unlike the other two engines, this engine showed local reduction in responses as the stiffness 228 Mn/m (13 x 10^6 lb/in) was increased. This can be related to the shift in modes, participation of other modes and damper excursion which is nonlinear with stiffness and damping.

Overall, the support deflection decreased as the stiffness increased (Figure 4.2-12). This trend, which was not observed in the other two engines, is again due to the shift in modes and participation of other modes in the total response.

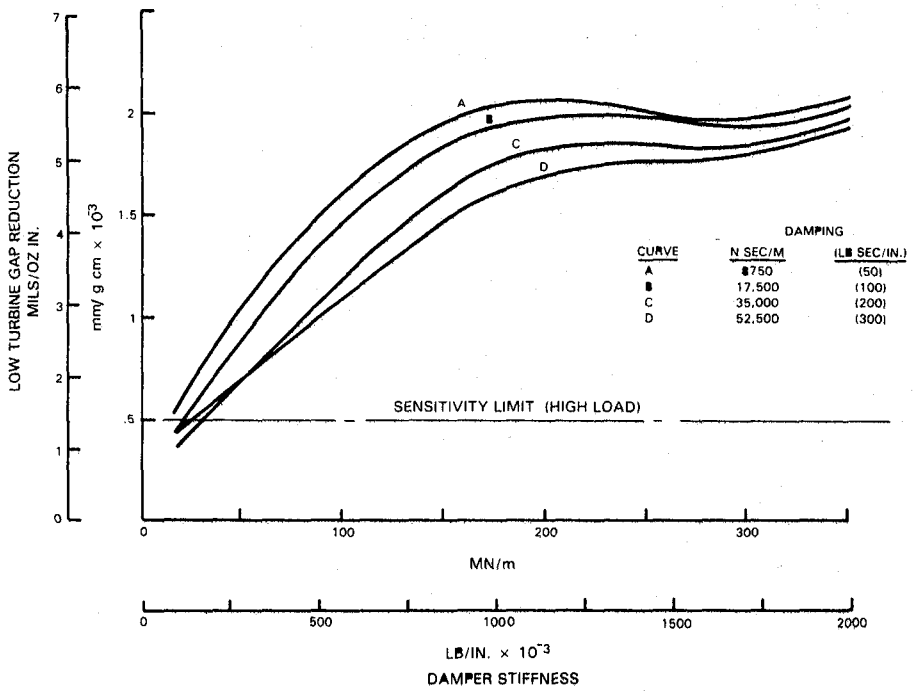

Figure 4.2-10 First Stage Turbine Gap Reduction Sensitivity; Military Engine

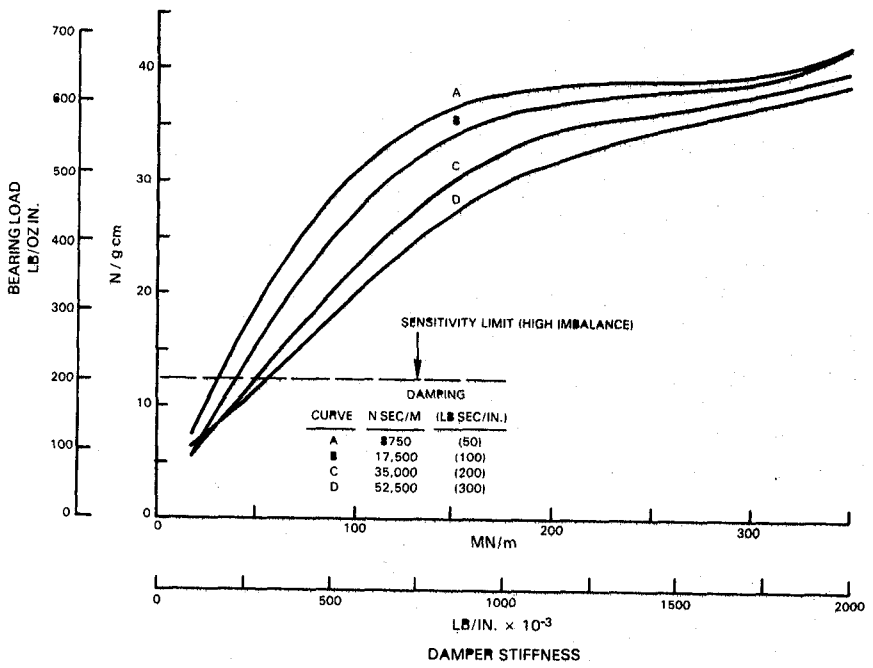

Figure 4.2-11 Number 5 Bearing Support Load Sensitivity; Military Engine

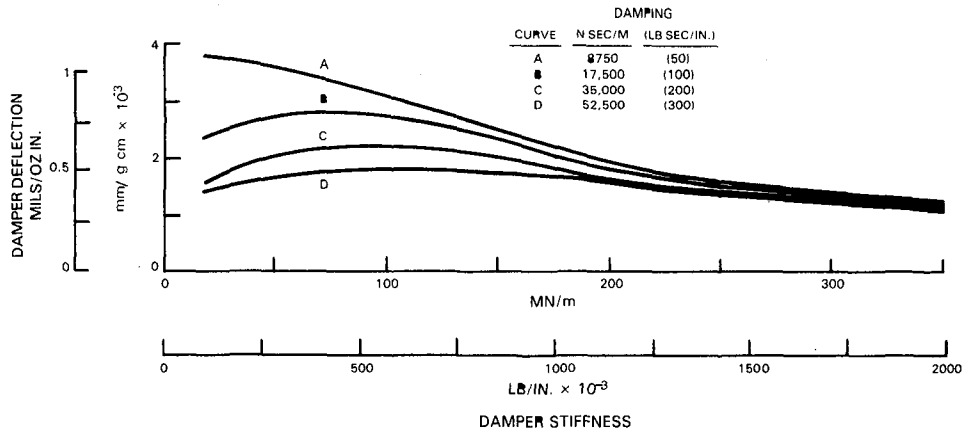

Figure 4.2-12 Support Deflection Response Sensitivities; Military Engine

From Figures 4.2-10 and 4.2-11, damper parameters can be selected to limit the turbine gap closure and support load. Then, a concept can be designed to obtain the selected parameters at damper amplitudes, as given in Figure 4.2-12. Details of damper parameters selected for the military engine are discussed in Section 5.2.3.

4.3 DAMPER ANALYSIS

Four high load damper concepts, multi-ring, cartridge, curved beam, and viscous/friction, were evaluated under high and low imbalance loads. For analytical purposes, the dampers were considered to be a combination of a spring and a viscous damper. The spring coefficient (K) is defined as the radial force per unit displacement, while the viscous damping coefficient (B) is defined as the tangential force per unit velocity of the shaft center (Reference 7). In a linear damper, these coefficients are constant: however, in a nonlinear damper they are functions of displacement. The forced response analysis used to evaluate damper performance can handle both linear and nonlinear (squeeze film) dampers. For squeeze film dampers, an iteration technique is used to obtain solution convergence.

Radial and tangential forces in the four concepts were determined, and corresponding stiffness (K) and damping (B) coefficients were defined. These coefficients were used to evaluate damper performance under imbalance loads.

All of the damper concepts except the curved beam damper are modifications of or variations on the conventional squeeze film damper. This type of damper is widely used and its performance and stiffness and damping characteristics are well understood. Since the analytical formulation of a squeeze film damper is common to three of the concepts studied, it is discussed in detail below.

The squeeze film damper generates damping and stiffness forces by shearing and squeezing the oil film. These forces can be determined by integrating the pressure solution of the Reynolds equation (Reference 8) which defines the

relationship between the oil velocities and the pressure distribution within the oil film. The form of the Reynolds equation and the corresponding solution depends on the type of damper, (i.e., long bearing approximation with negligible axial flow, short bearing approximation with negligible circumferential flow, or finite length approximation, which accounts for both axial and circumferential flows), and the magnitude of the oil supply pressure (References 9 and 10).

In this study, both the long and short bearing approximations were considered with either zero or very high supply pressure. The zero supply pressure results in a half-cavitated oil film, π film, and the high supply pressure assumes a supply pressure sufficient to suppress cavitation, 2π film. The resulting expressions for stiffness and damping, assuming circular centered whirl, are given in Table 4.3-I.

Table 4.3-I
Stiffness and Damping Expressions
for Short Bearing and Long Bearing Approximations

Type of Film	Short Bearing K	Short Bearing B	Long Bearing K	Long Bearing B
π film	$\frac{RL^3\mu\omega}{C^3}\ \frac{2\epsilon}{(1-\epsilon^2)^2}$	$\frac{RL^3\mu}{2C^3}\ \frac{\pi}{(1-\epsilon^2)^{3/2}}$	$\frac{R^3L\mu\omega}{C^3}\ \frac{24\epsilon}{(2+\epsilon^2)(1-\epsilon^2)}$	$\frac{R^3L\mu}{C^3}\ \frac{12\pi}{(2+\epsilon^2)(1-\epsilon^2)^{1/2}}$
2π film	0	$\frac{RL^3\mu}{C^3}\ \frac{\pi}{(1-\epsilon^2)^{3/2}}$	0	$\frac{R^3L\mu}{C^3}\ \frac{24\pi}{(2+\epsilon^2)(1-\epsilon^2)^{1/2}}$

4.3.1 Multi-Ring Damper

The basic shortcoming of the conventional squeeze film damper is that it provides insufficient clearance for rotor motion under high imbalance loads. The rotor support then becomes too stiff to allow efficient dissipation of energy. The multi-ring damper provides a method of circumventing this shortcoming. It is reported that the multi-ring damper has been used in turbochargers for diesel engines dating back at least to the 1930's.

Figure 4.3-1 shows the geometric arrangement of a two-film damper. Although there is no limit on the number of films, the two film damper is chosen here for analytical simplicity. Results which were obtained can be extended to any multi-ring damper.

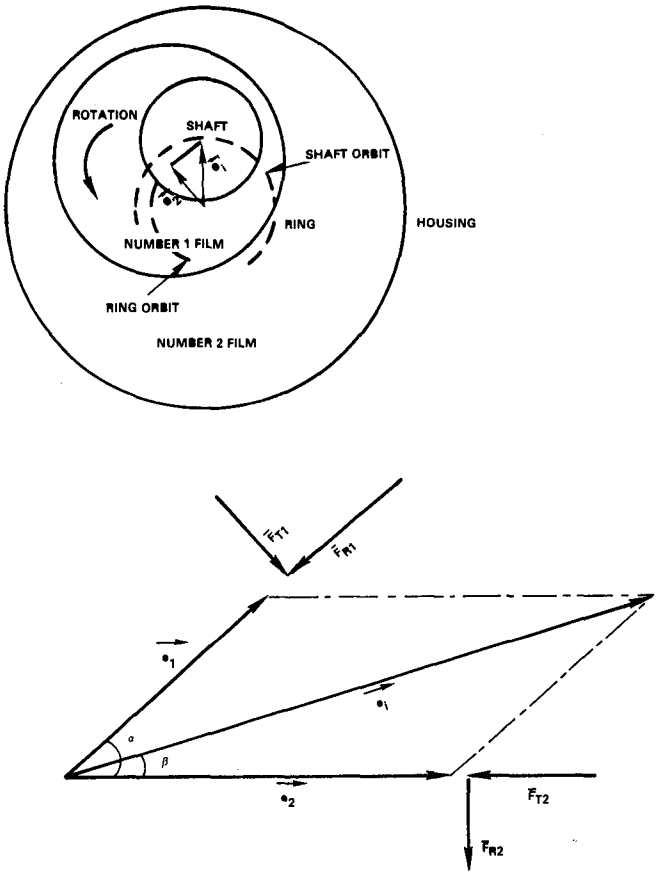

Figure 4.3-1 Geometric Arrangement of a Two-Film Damper

As the shaft whirls, the oil is sheared and squeezed, and hydrodynamic forces are generated in both films. These forces are dependent on shaft motion, ring motion, shaft position and ring position. If the shaft center moves by $\vec{e}_j$ and the ring center moves by $\vec{e}_R$, then shaft eccentricity with respect to the ring = $\vec{e}_1 = \vec{e}_j - \vec{e}_R$ and $\vec{e}_2 = \vec{e}_R$ = ring eccentricity.

In general $\vec{e}_1$ and $\vec{e}_2$ are not in phase (collinear). The phase angles α and β depend on the relative motion between the shaft and the ring. The hydrodynamic forces in the inner film can be represented by $\vec{F}_{R1}$ and $\vec{F}_{T1}$, while the hydrodynamic forces in the outer film can be represented by $\vec{F}_{R2}$ and $\vec{F}_{T2}$. Due to the inertia of the ring, the total force in the inner film is not equal to the total force on the outer film. For all practical purposes though, the inertial force can be neglected and the forces can be equated.

Eliminating the complex derivation, it can be shown that if the films are identical, and the shaft motion is synchronous and circular, then the ring is in phase with the shaft, i.e.:

$$\alpha = \beta = 0,\ \vec{e_1} = \vec{e_2},\ \vec{F}_{R1} = \vec{F}_{R2} \text{ and } \vec{F}_{T1} = \vec{F}_{T2}$$

Then, $e_j = e_1 + e_2$ = Total shaft eccentricity with respect to the housing

Now, for the inner film

$$\text{Stiffness} = K_1 = F_{R1}/e_1$$

and $$\text{Damping} = B_1 = F_{T1}/e_1\omega$$

Similarly for the outer film

$$\text{Stiffness} = K_2 = F_{R2}/e_2$$

and $$\text{Damping} = B_2 = F_{T2}/e_2\,\omega$$

Hence, the equivalent stiffness and damping of the two film dampers are:

$$K_{eq}\left(= \frac{F_{R1}}{e_j}\right) = \frac{F_{R2}}{e_j} = \frac{K_1}{2}\left(= \frac{K_2}{2}\right) = \frac{\text{Stiffness of one film}}{2}$$

$$B_{eq} = \frac{F_{T1}}{e_j}\left(= \frac{F_{T2}}{e_j}\right) = \frac{B_1}{2}\left(= \frac{B_2}{2}\right) = \frac{\text{Damping of one film}}{2}$$

Extending this approach to other multi-ring dampers, it can be shown that:

$$K_{eq} = \frac{\text{Stiffness of one film}}{n}$$

$$B_{eq} = \frac{\text{Damping of one film}}{n}$$

where n = Number of films.

Since the radial and tangential forces in a squeeze film damper are inversely proportional to the third power of the clearance, the stiffness and damping in a multi-film damper is n^2 times greater than the stiffness and damping of a single film damper of the same total clearance at the same eccentricity.

The advantage of a multi-ring damper lies in the fact that it provides sufficient stiffness and damping at high excursions. Small clearance can provide sufficient stiffness and damping, but the total excursion is limited by the small clearance. A large clearance damper can allow higher excursions, but the large clearance reduces stiffness and damping. Hence, the multi-ring damper is a compromise concept which provides high stiffness and damping at high excursions. Figure 4.3-2 illustrates the differences between 1) a small clearance, .13 mm (5 mils), single film damper; 2) a large clearance, .25 mm (10 mils), single film damper; and 3) two film, .13 mm (5 mils) each, multi-ring damper. It is assumed that the orbit is circular centered and that the two films are identical. The analysis is based on π film, long bearing approximation. As shown, the multi-ring damper provides four times higher stiffness and damping than a large clearance single film. The low clearance single film can also provide high stiffness and damping but only up to .13 mm (5 mils) of excursion. Note the rapid change in the stiffness and damping of the small clearance single film damper. This phenomena can cause the rotor to become unstable.

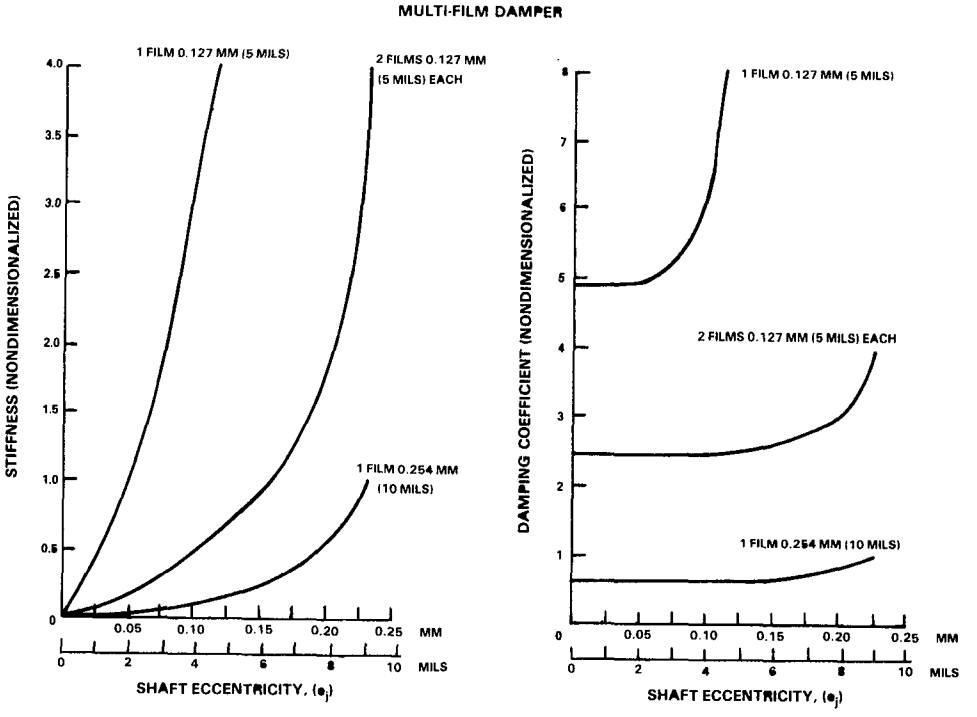

Figure 4.3-2 Stiffness and Damping Coefficients; Single Film and Multi-Ring Dampers

4.3.2 Cartridge Damper

This damper is similar in operation to the conventional squeeze film damper. However, it provides greater flexibility in selecting stiffness and damping for high and low load situations. It is a tightly sealed damper which allows use of a fluid other than bearing lubrication oil. In addition, the fluid can be sealed under pressure to alter damper performance. Stiffness and damping of the cartridge damper can be calculated by solving the Reynolds equation. The analytical formulation presented previously (Table 4.3-I) is also valid for the cartridge damper.

Figure 4.3-3 shows the difference between the conventional squeeze film damper and the cartridge damper. The stiffness and damping in a cartridge damper are higher due to the higher viscosity of the fluid. The π film, long bearing approximation for a circular centered orbit is assumed for analysis of the two non pressurized dampers. The pressurized damper is pressurized to suppress cavitation up to an eccentricity of 0.4. The pressurized cartridge damper shows reduced stiffness and increased damping. With proper selection of fluid pressure, this damper can be designed to provide required stiffness and damping over the entire operating range.

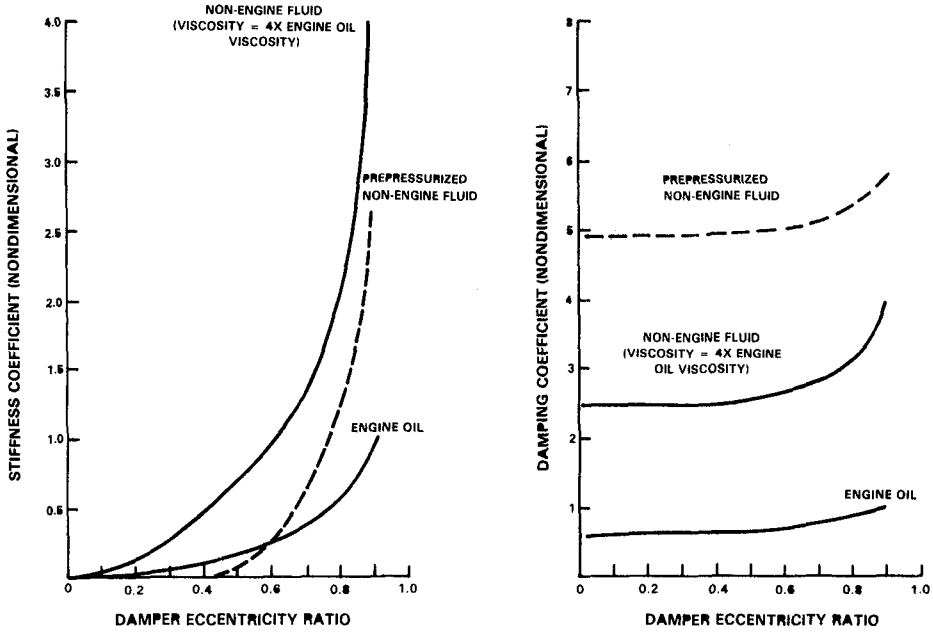

Figure 4.3-3 Comparison of Stiffness and Damping Coefficients; Cartridge Damper and Conventional Squeeze Film Damper

4.3.3 Curved Beam Damper

The serious drawback of any squeeze film damper is its nonlinear behavior at high eccentricities. This reduces its effectiveness as a vibration isolator at high amplitudes and loads. Although the multi-ring damper and cartridge damper are innovative designs aimed at alleviating this problem, they do not eliminate it completely. In addition to high rotor response and high support loads, nonlinearity can also cause instability in the system (Reference 11).

The curved beam damper which is patented by the Government Products Division of Pratt & Whitney Aircraft (Reference 12) reduces this nonlinearity significantly. It is possible to design the damper to be linear over its entire operating range of deflection and speed. With this concept (Figure 4.3-4) the curved beam(s) separate the inner housing from the outer housing. A recessed portion in the outer face of each spring forms a chamber of damper fluid. The radial restraint is derived from the stiffness of the beams while viscous damping is obtained from the pressure drop through the inlet/outlet ports (Reference 13).

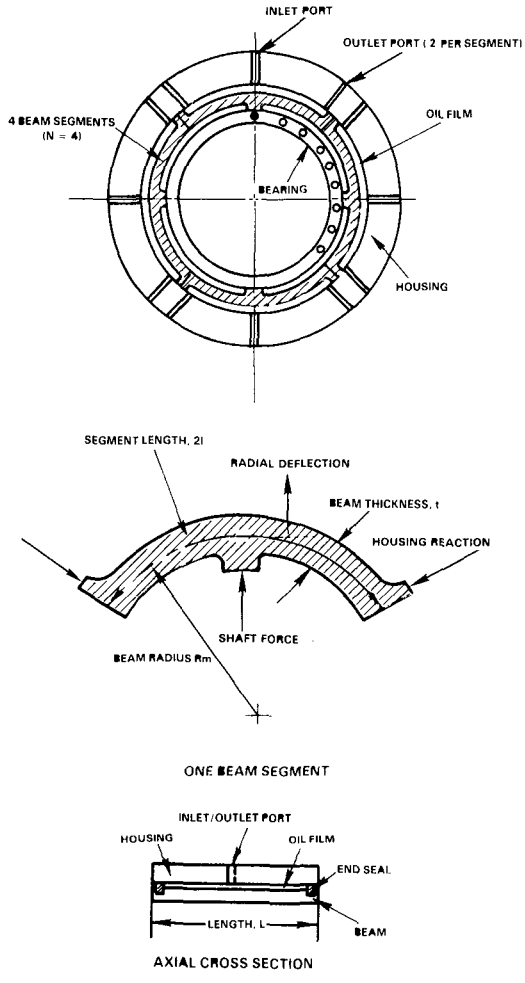

Figure 4.3-4 Curved Beam Damper

Analysis for Radial Stiffness (K)

The radial stiffness calculation is a two step process. In the first step, the force deflection characteristics of the beam are determined. In the second step, the total radial force acting on the shaft is calculated by taking into account the angular position of each beam with respect to the center of the shaft.

Force deflection characteristics are based on small deflection theory, which is linear over the deflection range. Beam geometry (length, curvature, thickness and width), end conditions (guided, fixed etc.) and material properties (Young's modulus) determine the force deflection characteristics while the number of beams determines the total effective stiffness in the system.

Assuming that the beams are segmented, (and thereby behave like a pin-pin beam) the force deflection characteristics can be given as:

$$\text{FORCE} \propto \frac{Et^3 Li}{Rm^3} \times \text{deflection}$$

$$\text{or Stiffness is proportional to } \frac{Et^3 L}{Rm^3}$$

If the number of segmented beams is N (Figure 4.3-4), then the effective total stiffness $(K) = A_1 \frac{Et^3}{Rm^3}$. Where A_1, the constant of proportionality, depends on the number of beams (N).

Analysis for Viscous Damping Coefficient (B)

In this concept, fluid is pumped through the supply and exhaust ports when shaft motion is transmitted to the curved beam. The total hydrodynamic pressure in the film is generated by two mechanisms; shearing the fluid within the clearance and pumping the fluid through the ports. The pressure generated by shearing the fluid can be modeled by the Reynolds equation and it is nonlinear. The pressure from pumping the fluid through the ports can be made proportional to the velocity of the fluid and it is linear. However, the nonlinear effect is minimized by using a relatively large clearance. Since the overall trend is to pump fluid back into the supply line, the outlet ports are kept small in order to maintain a uniform pressure distribution over the curved beam. The only purpose for the outlet port is to insure initial filling of the fluid cavity. Similarly, the supply pressure should be greater than the pressure drop in the port, otherwise the cavity will not be refilled and the starvation will occur.

The following steps are used to calculate the damping coefficient of the curved beam damper:

- o Knowing the velocity, eccentricity, clearance and port properties, pressure profile over the curved beam is calculated (both squeezing and pumping).

- o The forces acting on the beam are determined by integrating the profile over the area.

- o All the beam forces which are tangential to the shaft center are vectorially added.

- O The damping coefficient, i.e., tangential force per unit velocity, is calculated.

In the current study, nonlinearity is minimized by using a relatively large clearance damper and maintaining supply pressure above the port pressure drop, thereby avoiding starvation. In such instances, it can be shown that Tangential Force $\propto$ Port Flow Coefficient x Shaft Center Velocity x Beam Area.

If the port flow coefficient is constant over the operating range, then the tangential force is linearly proportional to the velocity and a constant coefficient of damping is obtained.

4.3.4 Viscous/Friction Damper

As described in Section 3.2.4, this is a dual damper. The small clearance viscous damper is effective at low levels of imbalance while the friction damper is effective at high loads. The additional energy dissipation due to friction and the tuned flexibility provided by the parallel support reduce rotor response.

The viscous/friction damper is designed around a predetermined threshold load level beyond which the friction force would be overcome and the friction damper activated. At very high loads the parallel support spring provides stiffness and coulomb damping becomes the predominant damping mechanism. For this study, it is assumed that at high load the viscous damper almost bottoms out and the operating eccentricity ratio is 0.9. This allows use of the viscous damper at high imbalance loads and recognizes the fact that theoretically the damper forces at an eccentricity ratio of 1.0 are infinite.

The friction damper is a constant force damper. The force which opposes the whirl motion is proportional to the normal clamping force on the plates (F_N). If the number of plates is m and the coefficient of friction is μ, then the frictional force is:

$$F_f = (m-1)\, F_n\, \mu$$

For a circular centered orbit, this force is tangential to the orbit. Thus the equivalent damping coefficient can be defined as:

$$C_f = \frac{F_f}{e\,\omega}$$ where e = orbit radius, ω = speed in rad/sec

As e, shaft orbit radius, increases, the coefficient decreases, resulting in a nonlinear damper. The stiffness of the friction damper is derived from the flexible support shown in Figure 3.2-4.

Under high load, the squeeze film and friction dampers are acting in series and the overall equivalent stiffness and damping is a function of the stiffness and damping of the individual components. Assuming that the inertia of the squeeze film and friction damper hardware is negligible, the equivalent stiffness and damping coefficient can be given as:

$$B_{equivalent} = \frac{(B_s K_f + K_s B_f)(K_f + K_s) - (K_s K_f - B_s B_f \omega^2)(B_s + B_f)}{(K_s + K_f)^2 + (B_s + B_f)^2 \omega^2}$$

and

$$K_{equivalent} = \frac{(K_s K_f - B_s B_f \omega^2)(K_s + K_f) + (B_s K_f + K_s B_f)(B_s + B_f)^2}{(K_s + K_f)^2 + (B_s + B_f)^2 \omega^2}$$

where:
K_f = Friction plate parallel support stiffness
K_s = Viscous damper stiffness
B_f = Friction damping
B_s = Viscous damping

At very high loads, the squeeze film damper is assumed to operate at an eccentricity ratio of 0.9, a ratio at which K_s and B_s are very high, i.e., $K_s \gg K_f$ and $B_s \gg B_f$. Then:

$$K_{equivalent} \cong K_f$$

$$B_{equivalent} \cong B_f$$

SECTION 5.0

RESULTS AND DISCUSSION OF RESULTS

Individual engine imbalance levels (low and high), corresponding absolute responses, and damper requirements were established for each engine. In addition, damper concepts were assessed and the most promising concepts evaluated under low and high imbalance loads. Results were compared with conventional squeeze film damper performance to assess the advantages of the high load damper concepts.

In general, a damper is designed for a particular application and condition. Hence, one damper cannot meet all of the dynamic requirements of an engine. In this study, damper requirements are established for specific engines and the most promising concept is used to meet these specific requirements. Basically, the following procedure was used to assess the applicability of a particular high load damper for a specific engine and evaluate its performance.

- Engine imbalance loads were defined.
- Engine response limits were defined.
- Damper requirements were determined.
- Damper concepts were evaluated and the most promising concept was selected
- The concept which was selected was evaluated for the defined imbalance loads and compared with conventional squeeze film dampers.

Results of this selection and evaluation are discussed below.

5.1 DAMPER OPERATING REQUIREMENTS

Damper requirements vary broadly depending on the class of the engine being considered. The three engine classes selected for the study, military, small general aviation and commecial, span a broad range of overall size, speed and thrust rating. As a result these engines have different levels of imbalance as well as different senstivities to imbalance and tolerance to resulting vibration. In addition each of the engine classes has different operating requirements which result in differing guidelines for satisfactory operation under vibratory conditions.

Each engine class has its own range of imbalances. Normal imbalance levels are low and depend on the tolerance stack up, trim balance capability and normal wear during operation. These imbalances are distributed over the entire engine. Experience with engine tests, flight data and various manufacturing and assembly procedures can determine the magnitude and location of distributed inherent imbalances in an engine. For analytical purposes, a single imbalance can be used and the corresponding engine response can be assumed to represent the response due to distributed imbalance.

High imbalance is accidental and most commonly caused by blade loss due to foreign object damage, severe operating conditions or premature fatigue failure. Experience with engine maintenance and flight data is used to determine the possibility of these accidental occurences. The effect of the high imbalance on the engine vibration depends on the size and location of the blade lost. For both the normal and high imbalance conditions the engine response limits are defined in terms of support loads and relative rotor to case deflections also known as gap reductions.

The requirements for safe operation and expected performance under high imbalance conditions differ for the three classes of engines. In commercial engines the emphasis is placed on maintaining component efficiency and minimizing the amount of hardware damage and repair costs later. The military engines must maintain thrust and performance for safe mission completion under extreme operating conditions. In general all three engines must maintain some required level of performance allowing safe operation of the aircraft to a selected destination. For this study the engine requirements are defined in terms of engine response under different imbalance. For example, the large transport engine can meet efficiency and repair requirements if compressor gap reductions and rubs are maintained below a certain level. This general approach to the specification of engine vibration limits is used for all three engines. Naturally, the requirements can be defined in terms of other parameters, such as stresses, slope, case deflections etc., but the procedure involved in selecting and assessing a damper would be similar to the procedure which is discussed here.

The high imbalance conditions considered in this study are limited to a turbine or compressor blade loss amounting to less than 3600 gm-cm (50 oz.in.). Current engines can be expected to operate safely under such conditions. Higher imbalances, e.g. fan blade loss, may occur and must be accounted for but engine operation for prolonged periods is not expected. Such extreme imbalance conditions are not considered here.

5.1.1 Large Transport Engine

The representative large transport engine has a high pressure compressor mode within the operating range. As described in Section 4.2-1, an imbalance at a compressor stage near the maximum amplitude location is more severe than an imbalance at any other location. It is assumed that 144 gm-cm or 2 oz-in of imbalance at the compressor simulates the normal imbalance in this engine. The engine response limit required to maintain efficiency or avoid rub is defined in terms of compressor deflection. A maximum gap reduction of .08 mm (3 mils) due to inherent imbalance is acceptable. Note that the normal clearance in large engines is .25 to .38 mm (10 to 15 mils), but factors such as thermal growth, maneuver deflection etc., reduce the operating clearance.

Experience has shown that single blade loss in a compressor is a common occurrence. Multi-blade loss and other types of imbalances related to foreign object damage have occurred, but these are unusual situations. Therefore, single blade loss imbalance of 3200 gm-cm (44 oz-in) is considered the high imbalance limit. Compressor deflection and damper support load limits are

established to define safety requirements. If the compressor deflection is less than 1.8 mm (70 mils) and the support load is less than 66700 N (15,000 pounds), structural integrity can be maintained and the engine can be shut down safely. The deflection limit is based on normal operating clearance and thickness of the abradable seal strip, while the load limit is based on stresses at critical locations.

In summary, the damper for the large transport engine should:

- o limit compressor gap reduction to .08 mm (3 mils) at 144 gm-cm (2 oz-in) of imbalance
- o limit compressor gap reduction to 1.8 mm (70 mils) at 3200 gm-cm (44 oz-in) of imbalance, and
- o limit the support load to 66700 N (15,000 lb) at 3200 gm-cm (44 oz-in) of imbalance.

From Figures 4.2-2 and 4.2-3 it can be seen that various combinations of stiffness and damping can meet these limits. Since this approach is based on linear extrapolation, some margin for nonlinearity is required. A stiffness of 88 Mn/n (500,000 lb/in) and damping of 53000 N-S/m (300 lb sec/in) can satisfy the limits with enough margin for any nonlinearity at high loads. For those damper parameters, the compressor deflection is .84 mm (33 mils) and the support load is 52800N (11900 lb) under high load balance. Both are within prescribed limits.

Figure 4.2-4 shows that the damper deflection for the selected stiffness and damping parameters is .56 mm or 22 mils under high load imbalance. In summary, the damper concept must provide stiffness of 88 MN/m (500,000 lb/in) and damping of 53000 N-S/m (300 lb sec/in) at an excursion of .56 mm (22 mils) in order to satisfy the high load limits. In addition, this damper must also meet low imbalance limits.

5.1.2 Small General Aviation Engine

The inherent imbalance in this engine can be simulated by a single imbalance load of 72 gm-cm (1 oz-in) at the turbine stage. For this inherent imbalance, the engine response limit is defined as .13 mm (5 mils) of gap reduction at the turbine stage, which guarantees smooth and efficient operation under normal imbalance. High load imbalance is a single blade loss at the turbine. Experience has shown that single blade loss at the turbine can occur. The establishment of a turbine mode within the operating range amplifies engine response to turbine blade loss many times. Safe shutdown limits are defined below.

The maximum allowable gap reduction should be less than 1.27 mm (50 mils). This includes normal operating clearance and the thickness of the rub strip. The turbine is prevented from contacting the case structure, which would result in catastrophic failure. The support load is also limited to 66700N (15,000 lbs) in order to assure structural integrity and avoid further damage.

Hence, the damper concept for the small general aviation engine should meet the following criteria.

- o limit turbine deflection to .13 mm (5 mils) at 72 gm-cm (1 oz-in) of imbalance
- o Limit turbine deflection to 1.27 mm (50 mils) under blade loss imbalance of 720 gm-cm (10 oz-in), and
- o limit the support load to 66700 N (15,000 lbs) under blade loss imbalance of 720 gm-cm (10 oz-in).

From Figures 4.2-6 and 4.2-7 it can be seen that a stiffness of 35 MN/m (200,000 lb/in) and damping of 26000 N-S/m (150 lb sec/in) can meet these limits. Using these stiffness and damping values under blade loss conditions, the turbine deflection and support load will be 1.02 mm (40 mils) and 22700 N (5100 lbs) respectively. These deflections are within the set limits. A damper excursion of .53 mm (21 mils) is required to dissipate enough energy to maintain deflection and load within limits. Linear extrapolation also ensures safe operation at low levels of imbalance (deflection = .10 mm (4 mils)). Although there is sufficient margin in the support load, the deflection margin may be inadequate if the damper is highly nonlinear.

5.1.3 Military Engine

The military engine has a different design approach to safety requirements than the commercial engine. Still, it is assumed that these requirements can be defined in terms of deflections and loads at critical locations. As described previously, the military engine has a low pressure turbine mode within the operating range. Inherent imbalance and corresponding engine response can be simulated by a single imbalance in the turbine. Similarly, a high imbalance is represented by a single blade loss at the turbine. If turbine deflection and support loads are maintained within design limits, it is predicted that engine will meet its safety and performance criteria. Detailed requirements are as follows:

- o At low imbalance (144 gm-cm (2 oz-in) at the turbine), the deflection should be 0.13 mm (5 mils)
- o At high imbalance, (single blade loss, or 3600 gm-cm (50 oz-in), the deflection should be equal to or less than 1.18 mm (70 mils) and load should be equal to or less than 44500 N (10,000 lbs).

The deflection limit at high load prevents turbine failure and assures a safe level of thrust, while the support load limit guarantees structural integrity.

Figures 4.2-10 and 4.2-11 show that a stiffness of 18 MN/m (100,000 lb/in) and damping of 35000 N-S/m (200 lb sec/in) can just meet the deflection limits and that any change in those parameters may result in undesirable failures. The load limit is easily satisfied; therefore the damper concept has to provide 18 MN/m (100,000 lb/in) stiffness and 35000 NS/m (200 lb sec/in) damping at high imbalance loads. The damper should also allow for 0.57 mm (22.5 mils) of excursion (Figure 4.2-12) for efficient dissipation of vibrational energy.

This concept should also limit low imbalance deflection to assure efficient engine operation.

Table 5.1-I summarizes the low and high load limits, damper requirements and expected engine response at low and high loads for the three engines.

Table 5.1-I

High and Low Load Damping Limits, Damper Requirements, and Expected Engine Response at High and Low Loads

Parameter	Large Transport Engine	Small General Aviation Engine	Military Engine
Low Imbalance gm cm (oz-in)	High Pressure Compressor 144 (2)	Turbine 72 (1)	Low Pressure Turbine 144 (2)
Low Response mm (mils)	HPC Gap Reduction 0.08 (3)	Turbine Gap Reduction 0.13 (5)	LPT Gap Reduction 0.13 (5)
High Imbalance gm cm (oz-in)	High Pressure Compressor 3200 (44)	Turbine 720 (10)	Low Pressure Turbine 3600 (50)
High Response Limit mm (mils)	HPC Gap Reduction 18 (70)	Turbine Gap Reduction 1.3 (50)	LPT Gap Reduction 1.8 (70)
Maximum Support Load Limit N (lbs)	Number 2 Support 67,000 (15,000)	Number 3 Support 67,000 (15,000)	Number 5 Support 45,000 (10,000)
Required Stiffness MN/m (lb/in)	88 (500,000)	35 (200,000)	18 (100,000)
Required Damping NS/m (lb sec/in)	53,500 (300)	26,300 (150)	35,000 (200)
Required Damper Excursion mm (mils)	0.56 (22)	0.53 (21)	0.57 (22.5)

5.2 SELECTED DAMPER CONCEPTS

Damping requirements for the representative engines can be met by designing damper systems which limit engine response under high and low imbalance loads. Multi-ring, cartridge, curved beam and viscous/friction dampers were assessed. Detailed designs were developed to meet damping requirements for each engine.

The cartridge damper is a tightly sealed squeeze film damper in which a fluid other than engine lubrication oil is used. The fluid can be prepressurized to suppress cavitation. It was felt that consideration of this damper as a separate concept would not add to the technical content of the program. A cartridge damper is basically a conventional damper and conventional dampers are already well understood for engineering purposes. In addition, the need for an external heat dissipation mechanism and the difficulty in designing perfectly sealed hardware make this concept an unacceptable solution. Therefore the cartridge damper concept was eliminated from further consideration.

The remaining damper concepts were individually analyzed for application to the representative engines. An iterative design procedure was followed until an acceptable geometry for the concept was developed. This geometry provided the required high load damping and stiffness for the specific engine application while meeting physical constraints, such as bearing size and flow path dimensions. In some cases, more than one physical configuration was found to be satisfactory, while in others no satisfactory configuration was developed. The final configurations described in Table 5.2-1 and discussed in Sections 5.2.1, 5.2.2 and 5.2.3 were selectd based on keeping dimensions within reasonable limits for the particular applications and providing greatest linearity over the required displacement range. The configurations which were selected were not necessarily optimized in every detail.

The criteria for selection of the final concept for each engine considers practicality of design, linearity and size. The concepts and their acceptability are discussed in the following sections.

5.2.1 Large Transport Engine

Multi-Ring Damper -- Different configurations were considered, including two film and three film dampers with axially sealed and open cavities. The final configuration was a single film with a parallel spring support. This limiting case of the multi-ring damper resulted because the large diameter required for this application allows the single film to provide sufficient damping even at the large clearance required for displacement under high load conditions. Any attempt to go to multiple oil films resulted in an increase of the damping and stiffness beyond the required levels. Physical geometry and assumed operating conditions for this damper are given in Table 5.2-1. At high load, the operating eccentricity ratio was assumed to be approximately 0.75. For compatibility, the radius and length were kept the same as the bearing dimensions. Preliminary calculations showed that this configuration can meet engine response limitations at low and high imbalance loads.

Curved Beam Damper -- Theoretically, the curved beam damper can be designed for any application; the limiting parameters are required beam size and port flow coefficients. The independent stiffness and damping characteristics of the curved beam damper eliminate the common difficulty encountered in designing a squeeze film damper. A four beam damper was developed for this engine. Details of the geometry and operating conditions needed to generate required stiffness and damping are given in Table 5.2-I.

Table 5.2-I

Damper Geometry and Operating Conditions

Damper Concepts	Large Transport Engine	Small General Aviation Engine	Military Engine
Multi-Ring			
Number of Films	One	Three	
Radial Clearance mm (mils)	0.75 (29)	0.28 (11)	
Maximum Eccentricity Ratio	0.75	0.67	
Cavitation	Pi Film	Pi Film	
Type of Film	Axially Sealed	Axially Sealed	None
Parallel Support MN/m (lb/in)	44 (2.5 x 10^5)	26 (1.5 x 10^5)	
Radius cm (in)	16.5 (6.5)	7.6 (3)	
Length cm (in)	5.1 (2.0)	2.5 (1)	
Viscosity of Oil cp (Reyn)	6.9 (1 x 10^{-6})	6.9 (1 x 10^{-6})	
K at High Load MN/m (lb/in)	86 (4.91 x 10^5)	44 (2.2 x 10^5)	
B at High Load NS/m (lb sec/in)	74,400 (425)	24,000 (135)	
K at Low Load MN/m (lb/in)	47 (2.68 x 10^5)	30 (1.7 x 10^5)	
B at Low Load NS/m (lb sec/in)	74,400 (425)	24,000 (135)	
Curved Beam			
Number of Beams	4	4	4
Thickness of Beam cm (in)	4.0 (1.59)	0.795	0.430
Oil Cavity Thickness mm (mils)	1.02 (40)	0.64 (25)	0.64 (25)
Supply Pressure N/m^2 (PSI)	1.1 x 10^6 (155)	1.6 x 10^6 (232)	2.0 x 10^6 (285)
Port Pressure Drop N/m^2 (PSI)	1.2 x 10^6 (170)	1.7 x 10^6 (247)	2.1 x 10^6 (300)
Film Pressure N/m^2 (PSI)	1.6 x 10^5 (23)	3.5 x 10^5 (50)	1.7 x 10^5 (25)
Port-Flow Coefficient	0.56	0.26	0.18
Maximum Bending Stress N/m^2 (PSI)	2.0 x 10^8 (28,200)	2.4 x 10^8 (35,400)	2.5 x 10^8 (36,600)
Radius cm (in)	16.5 (6.5)	10.2 (4)	7.6 (3)
Length cm (in)	5.1 (2.0)	3.8 (1.5)	5.1 (2)
K at High Load and K at Low Load MN/m (lb/in)	88 (5 x 10^5)	35 (2 x 10^5)	18 (1 x 10^5)
B at High Load and B at Low Load MN/m (lb/in)	52,500 (300)	26,300 (150)	35,000 (200)
Viscous/Friction			
Radius cm (in)	16.5 (6.5)	7.6 (3)	7.6 (3)
Length cm (in)	5.1 (2.0)	2.5 (1)	5.1 (2)
Viscous Damper Radial Clearance mm/(mils)	0.13 (5)	0.13 (5)	0.13 (5)
Type of Cavity	Axially Open	Axially Open	Axially Open
Cavitation	Pi Film	Pi Film	Pi Film
Viscosity of Oil cp (Reyns)	6.9 (1 x 10^{-6})	6.9 (1 x 10^{-6})	6.9 (1 x 10^{-6})
Normal Load N (lb)	8540 (3800)	6680 (2970)	7150 (3180)
Number of Plates	7	7	7
Coefficient of Friction	0.15	0.15	0.15
Parallel Support MN/m (lb/in)	88 (5 x 10^5)	35 (2 x 10^5)	18 (1 x 10^5)
K at High Load MN/m (lb/in)	85 (4.83 x 10^5)	32 (1.8 x 10^5)	17 (9.8 x 10^4)
B at High Load NS/m (lb sec/in)	51,000 (289)	21,000 (119)	34,200 (195)
K at Low Load MN/m (lb/in)	22 (1.25 x 10^5)	20 (1.13 x 10^5)	19 (1.1 x 10^5)
B at Low Load NS/m (lb sec/in)	122,000 (695)	15,000 (86)	26,300 (150)

The large clearance oil cavity minimizes nonlinear effects from squeezing and shearing. The high supply pressure eliminates oil starvation. It is assumed that the oil in the clearance cavitates during expansion, thereby maintaining a constant film pressure (-1.03 x 10^5 N/m^2 or -15 psia). Note that the beam is very thick. More beams might reduce beam thickness, but they would adversely affect bending stresses (it is assumed that the beams are steel) and inlet port flow coefficients. The parametric analysis conducted in this program showed that the curved beam damper can meet low and high load requirements.

Viscous/Friction Damper -- Design of this concept, which consists of two dampers in series, was based on the following assumption: the viscous damper (which is a conventional squeeze film damper) controls the low loads, while the high loads are primarily controlled by the friction damper. Various clearances and friction damper geometries were investigated to obtain required stiffness and damping at low and high excursions. One configuration which meets this requirement is shown in Table 5.2-I. The 0.13 mm (5 mils) squeeze film damper controls low vibration due to inherent imbalance while the friction damper, once actuated, can dissipate enough energy to control high vibrations which could occur under blade loss. This configuration also required a parallel support of 88MN/m (5×10^5 lb/in). Although various design configurations are feasible, no attempt was made to develop an optimized design.

All three concepts were candidates for the large transport engine. Each concept could be designed to meet the low and high imbalance response limits of the engine; but the practicality, size and weight, maintenance and previous experience associated with each concept decided the relative advantage of one concept over the others. Of the three concepts, only the single squeeze film damper is used successfully in an engine. On the other hand, the curved beam and the viscous/friction dampers are still being evaluated on test rigs. This and the following considerations made the single film damper the most promising concept for further evaluation in a large transport engine:

- The risks associated with a single film damper are minimum.
- The large transport engine is insensitive to small nonlinearity which is inherent in the squeeze film damper.
- The curved beam damper which is linear and compact did not offer any significant advantages in this engine. In addition, the designed thickness of the beam might be too large for practical application.
- The viscous/friction damper is very nonlinear and occupies large space. It also has more moving compartments which result in high maintenance requirements. In addition, an effective friction-heat removal system is needed in such dampers.

5.2.2 Small General Aviation Engine

Multi-Ring Damper -- After iterations on two and three film dampers, a multi-ring damper configuration with a parallel support was developed (see Table 5.2-I). The axially sealed three film damper seemed to provide sufficient energy dissipation and control over engine response at low and high imbalance loads. The radius and length of the damper were close to the bearing dimensions. This 0.84 mm (33 mil) clearance damper was assumed to operate at an eccentricity ratio of 0.67 at high imbalance loads.

Curved Beam Damper -- Once again, a four beam damper was used to obtain required stiffness and damping coefficients. The physical dimensions and operating conditions are shown in Table 5.2-I. The 0.64 mm (25 mils) radial clearance minimizes nonlinearity due to pressures generated by squeezing and shearing the oil. The high supply pressure avoids starvation.

Viscous/Friction Damper -- The geometry and operating conditions of the viscous/friction damper are shown in Table 5.2-I. This configuration can generate sufficient stiffness and damping at low and high excursions, and control engine deflections and support loads. A parallel support of 35 MN/m (2×10^5 lb/in) is required to provide sufficient stiffness at high load. The viscous damper is active at low levels of vibration while the friction damper is assumed to play a dominant role under high imbalance loads.

All three concepts were candidates for the small general aviation engine. Each concept could be designed to meet the low and high imbalance response limits of the engine. The curved beam damper is small in size and provides a linear stiffness and damping. The size of the engine and its sensitivity to nonlinear stiffness and damping were considered and the curved beam damper was selected as the most promising concept for further evaluation. The other two concepts were not considered for the following reasons.

- Multi-ring with parallel support and viscous/friction dampers are heavy and require too much space for this application.
- Engine sensitivity to nonlinear stiffness and damping also discouraged use of multi-ring and viscous/friction dampers.
- The curved beam damper offered the lowest weight and size for this engine.

5.2.3 Military Engine

Multi-Ring Damper -- Even after several iterations, no satisfactory configuration could be designed. Single film, two film and three film designs with different operating conditions were evaluated, but none could meet low and high load requirements satisfactorily.

Curved Beam Damper -- The geometry and operating conditions of the curved beam damper are described in Table 5.2-I. This configuration, which is not unique in any way, can generate the required stiffness and damping and maintain engine response below limits for safe operation. Once again, a large clearance was used to minimize nonlinear effects. In addition, supply pressure was selected to avoid starvation.

Viscous/Friction Damper -- Assuming that the viscous damper controls low vibrations and the friction damper controls high vibrations, the geometry and operating conditions needed to meet damping requirements are shown in Table 5.2-I. A parallel support of 18 MN/m (1×10^5 lb/in) was required to provide sufficient stiffness at high load.

Unlike the other two engines, only two concepts could be designed for the military engine. The curved beam and viscous/friction concepts were potential candidates for this engine. Out of these two, the curved beam damper was considered to be the most promising one for the military engine. This and the following reasons were considered before the curved beam damper was chosen for further evaluation:

- The military engine is sensitive to small changes in the stiffness and damping. Hence use of viscous/friction damper might result in unacceptably high engine response and support loads.

- Viscous/friction damper, in addition to its large size, is mechanically complex with moving parts subject to wear and potentially in need of periodic maintenance.

To summarize, several concepts could be considered potential candidates for each representative engine. The curved beam damper was selected as the most promising concept for the military and small general aviation engines while a large clearance single film damper with parallel support was selected for the large transport engine.

5.3 PREDICTED PERFORMANCE

The most promising damper concepts for all three engines have been selected and designed. The engines did not have any dampers in their bill of material form, but the introduction of a sensitive mode within the operating range created a requirement for a damper that would at least control low inherent imbalance. It was also shown during damper selection that a conventional damper of 0.13 mm (5 mils) clearance can meet the low load requirements for all three engines. Therefore, it is assumed that the three representative engines would have the 0.13 mm (5 mils) conventional damper for baseline response. The new proposed concepts have been evaluated against this baseline response.

The forced response analysis used in this study can consider a squeeze film damper by iteration on nonlinear stiffness and damping. The curved beam damper was analyzed as a constant stiffness and damping element.

Results of the response analyses for these engines are discussed below.

5.3.1 Large Transport Engine

The large clearance, single film damper with a parallel support was considered to be the most promising concept for the large transport engine. The engine was analyzed with this damper and a conventional damper for low, intermediate and high levels of imbalance. Figure 5.3-1 shows the compressor gap reductions as well as the limits for safe operation. At low load (144 gm-cm (2 oz-in)), engine responses with the proposed and conventional dampers were small and within limits for efficient operation.

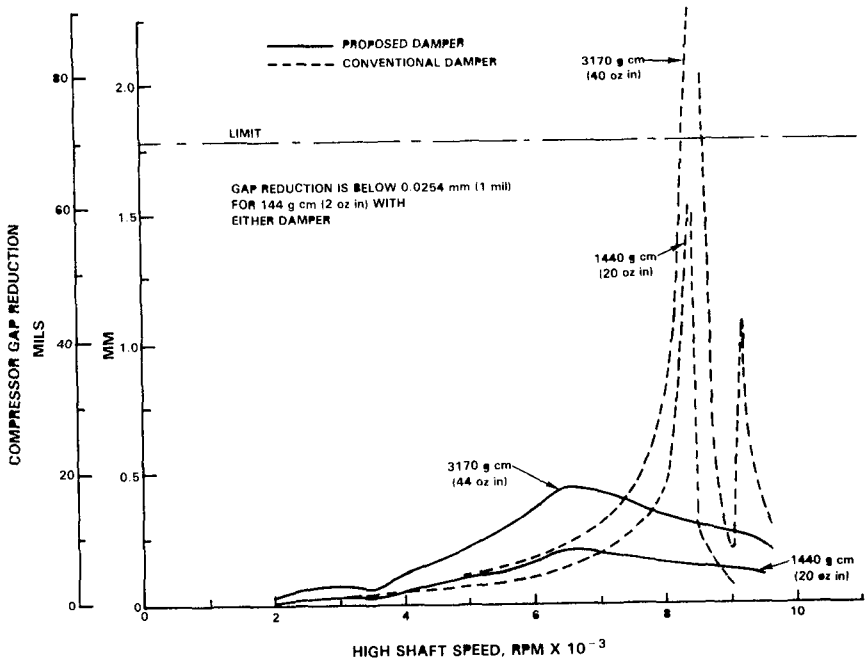

Figure 5.3-1 Compressor Gap Reduction at Low, Intermediate, and High Levels of Imbalance; Conventional and Proposed Dampers; Large Transport Engine

The proposed damper reduced the gap by a maximum of 0.018mm (0.7 mil) while the conventional damper reduced it by a maximum of 0.01 mm (0.4 mil). The limit was 0.08 mm (3 mils). Hence, both dampers were effective at low loads and maintained the deflection levels well within design values. The high load 3200 gm-cm (44 oz-in) response was noticeably different. The proposed damper held the compressor gap reduction to less than 0.45 mm (18 mils) throughout the operating range, compared to the design limit of 1.8 mm (70 mils). This control was due to the availiability of higher than necessary damping at the desired stiffness. Nonlinearity also might have contributed to this reduction; the proposed damper is overdesigned and reduction in damper clearance might be possible. Lower clearance dampers are advantageous in meeting maneuver deflection criteria.

The conventional squeeze film damper could not meet the high load requirements. The maximum gap reduction was 5.8 mm (228 mils) which exceeded safe shutdown limits. Even at an intermediate level of imbalance 1440 gm-cm (20 oz-in), the maximum gap reduction was as high as 1.5 mm (60 mils).

Based on linear analysis, the expected peak response speed was 6400 rpm. Surprisingly it is very close to the peak response speed for the proposed damper, but it is off for the conventional damper. Interestingly, the

conventional damper introduced another peak within the operating range which was not observed in the engine with the proposed damper. The high nonlinearity at high operating eccentricity might have caused the shift in modes and the change in coupling between modes.

Figure 5.3-2 shows the load transmitted through the damper support. Although the limit was very high (approximately 66,700 N (15,000 lbs)), the conventional damper showed a load of 833000 N (187,300 lbs) at high imbalance loads (not shown in figure). The support load was 271000 N (47,480 lbs) at intermediate load (1440 gm-cm (20 oz. in)). Unlike the compressor gap reduction response, the bearing load showed two peaks in the operating range even with the proposed damper.

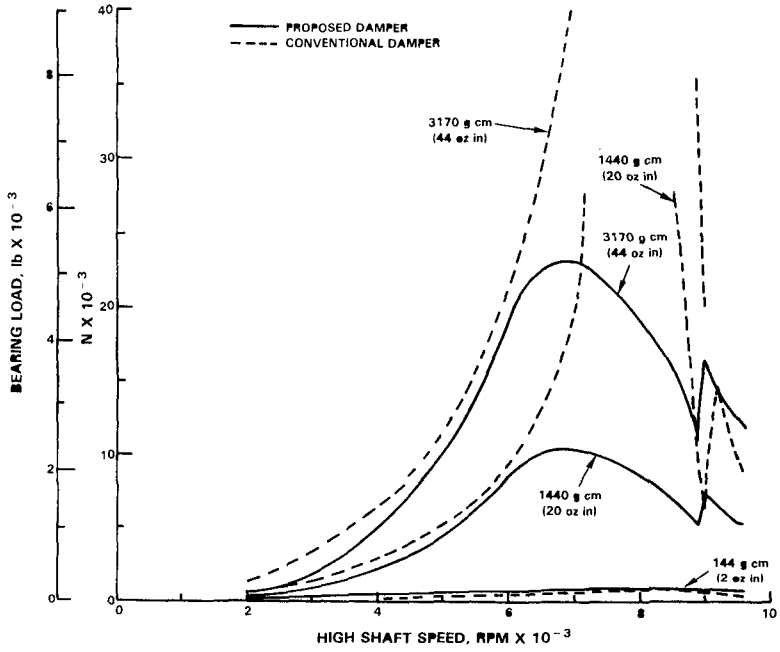

Figure 5.3-2 Number 2 Bearing Loads; Conventional and Proposed Dampers; Large Transport Engine

Table 5.3-I describes peak responses at various locations for the engine with the proposed damper. In comparison with the responses in Table 5.3-II for the conventional squeeze film damper, the proposed damper showed better overall performance for moderate and high imbalance. However the conventional damper showed better performance at low imbalance because it was designed specifically for these conditions.

Table 5.3-I
Large Transport Engine Response; Proposed Damper
(0.74 mm, parallel supported damper)

Response Location	Imbalance 144 gm-cm		1440 gm-cm		3200 gm-cm	
HPC Stage 1 Gap Reduction mm (mils)	0.015	(0.6)	0.17	(6.5)	0.41	(16.1)
HPC Stage 3 Gap Reduction	0.018	(0.7)	0.18	(7.2)	0.46	(18.0)
HPC Stage 5 Gap Reduction	0.018	(0.7)	0.19	(7.3)	0.46	(18.0)
HPC Stage 7 Gap Reduction	0.018	(0.7)	0.19	(7.3)	0.46	(18.1)
HPC Stage 9 Gap Reduction	0.018	(0.7)	0.18	(7.0)	0.44	(17.5)
HPC Stage 11 Gap Reduction	0.015	(0.6)	0.17	(6.5)	0.41	(16.2)
HPT Stage 1 Gap Reduction	0.013	(0.5)	0.13	(5.3)	0.30	(11.8)
HPT Stage 2 Gap Reduction	0.015	(0.6)	0.15	(6.1)	0.34	(13.5)
Support Number 2 Deflection	0.013	(0.5)	0.13	(5.3)	0.33	(12.8)
Support Number 3 Deflection	0.003	(0.1)	0.02	(0.8)	0.05	(2.0)
Fan Case Deflection	0.025	(1)	0.25	(10)	0.57	(22.4)
Fan Duct Deflection	0.008	(0.3)	0.08	(3.0)	0.17	(6.6)
Turbine Case Deflection	0.005	(0.2)	0.04	(1.7)	0.97	(3.8)

Table 5.3-II
Large Transport Engine Response; Conventional Squeeze Film Damper
(0.13 mm damper)

Response Location	Imbalance 144 gm-cm		1440 gm-cm		3200 gm-cm	
HPC Stage 1 Gap Reduction mm (mils)	0.010	(0.4)	0.81	(32.0)	2.89	(114.0)
HPC Stage 3 Gap Reduction	0.010	(0.4)	1.37	(54.0)	5.18	(204.0)
HPC Stage 5 Gap Reduction	0.010	(0.4)	1.52	(60.0)	5.79	(228.0)
HPC Stage 7 Gap Reduction	0.010	(0.4)	1.65	(65.0)	6.40	(252.0)
HPC Stage 9 Gap Reduction	0.010	(0.4)	1.68	(66.0)	6.53	(257.0)
HPC Stage 11 Gap Reduction	0.010	(0.4)	1.57	(62.0)	6.17	(243.0)
HPT Stage 1 Gap Reduction	0.005	(0.2)	0.18	(6.9)	0.66	(26.0)
HPT Stage 2 Gap Reduction	0.005	(0.2)	0.46	(18.0)	1.73	(68.0)
Support Number 2 Deflection	0.008	(0.3)	0.11	(4.3)	0.12	(4.8)
Support Number 3 Deflection	0.001	(0.04)	0.07	(2.9)	0.28	(11.0)
Fan Case Deflection	0.002	(0.06)	0.48	(19.0)	2.16	(85.0)
Fan Duct Deflection	0.002	(0.08)	0.33	(13.0)	1.32	(52.0)
Turbine Case Deflection	0.002	(0.06)	0.04	(1.5)	0.12	(4.9)

5.3.2 Small General Aviation Engine

The curved beam damper was selected as the most promising concept for the small general aviation engine. The engine, which is sensitive to imbalance load and changes in stiffness, was analyzed with the curved beam (proposed) damper and a 0.13 mm (5 mils) radial clearance conventional squeeze film damper. Figure 5.3-3 shows the turbine gap reduction as well as the design limits for safe shutdown. The limits for low imbalance loads were met by both dampers. In fact, the conventional damper was more effective at low inherent imbalance 72 gm-cm (1 oz-in). Gap reduction with the conventional damper was 0.05 mm (2 mils) while gap reduction with the curved beam damper was 0.13 mm (5 mils). In addition, a single peak was seen for the curved beam damper, but the response was almost flat for the conventional damper.

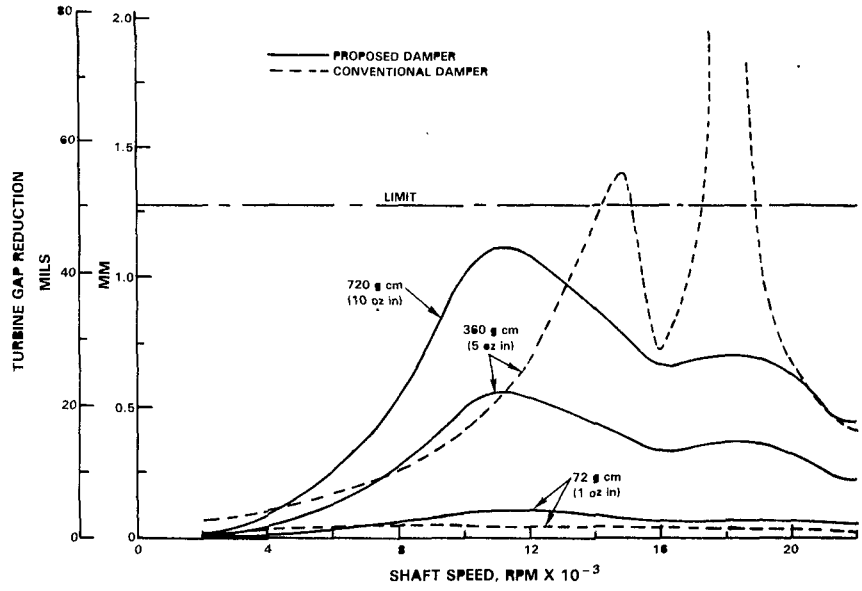

Figure 5.3-3 Turbine Gap Reduction at Low, Intermediate, and High Levels of Imbalance; Conventional and Proposed Dampers; Small General Aviation Engine

At high imbalance 720 gm-cm (10 oz-in), the curved beam damper maintained the gap reduction within the limit as expected. At the same time, it introduced another peak within the operating range. In contrast, the conventional damper could not meet the high load limits. Even at an intermediate level of imbalance 360 gm-cm (5 oz-in), the gap reduction was 3.33 mm (131 mils), which exceeded the safety limits. Nonlinearity, high stiffness and damping caused the shift of peak response speeds.

Figure 5.3-4 shows the support load at the damper location. The proposed damper held the load well below the design limit, but the conventional damper did not. Even at the intermediate imbalance level, the load was 146800 N (33,000 lbs), which is above the allowable limit for this application.

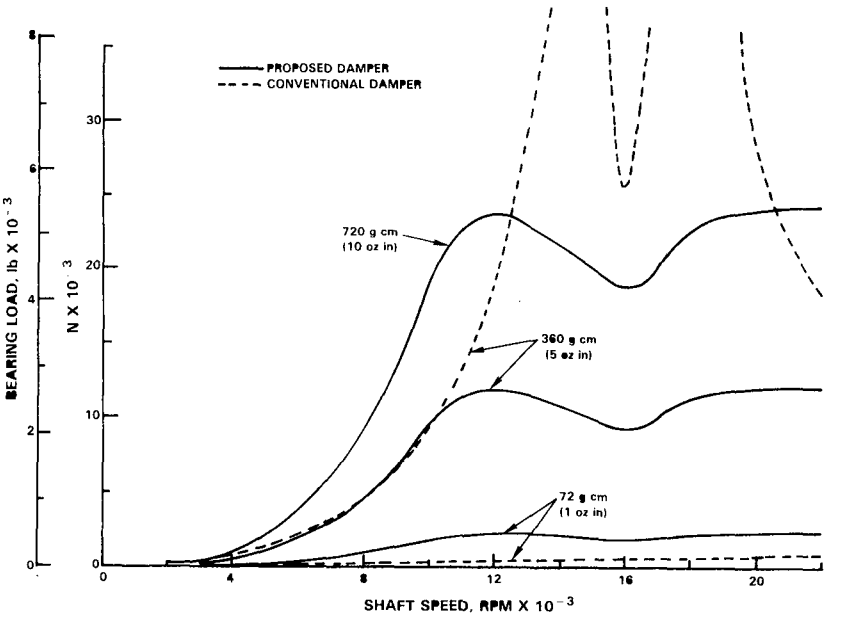

Figure 5.3-4 Number 3 Bearing Loads; Conventional and Proposed Dampers; Small General Aviation Engine

The overall response of the engine with the proposed damper is shown in Table 5.3-III. In comparison with the response for the conventional damper (Table 5.3-IV), the proposed damper showed siginificantly better performance for intermediate and high imbalance loads. However, the conventional damper showed better performance at low loads because it was designed specifically for those conditions.

The response for the curved beam damper at intermediate levels of imbalance can be obtained by linearly scaling the response at low imbalance. This is because the curved beam damper is linear over its operating range.

For the conventional squeeze film damper, the engine response exceeded the defined designed limits at intermediate levels of imbalance. Therefore the responses at high imbalance loads were not presented.

Table 5.3-III

Small General Aviation Engine Response; Proposed Damper
(Curved beam)

Location	Imbalance 72 gm-cm		Imbalance 722 gm-cm	
Compressor Stage 1 Gap Reduction mm (mils)	0.023	(0.9)	0.23	(8.9)
Compressor Stage 3 Gap Reduction	0.028	(1.1)	0.29	(11.3)
Compressor Stage 5 Gap Reduction	0.030	(1.2)	0.32	(12.4)
Compressor Stage 7 Gap Reduction	0.033	(1.3)	0.33	(12.9)
Support Number 1 Deflection	0.015	(0.6)	0.16	(6.2)
Support Number 2 Deflection	0.023	(0.9)	0.22	(8.8)
Support Number 3 Deflection	0.051	(2.0)	0.50	(19.8)
Case Deflection 1 (Front)	0.025	(1.0)	0.25	(10.0)
Case Deflection 2 (Bearing Number 2)	0.020	(0.8)	0.21	(8.4)
Case Deflection 3 (Bearing Number 3)	0.025	(1.0)	0.25	(10.0)
Case Deflection 4 (End)	0.053	(2.1)	0.54	(21.3)
Turbine Stage 1 Gap Reduction	0.089	(3.5)	0.90	(35.4)
Turbine Stage 2 Gap Reduction	0.114	(4.5)	1.13	(44.5)

Table 5.3-IV

Small General Aviation Engine Response; Conventional Damper
(0.13 mm squeeze film)

Location	Imbalance 72 gm-cm		Imbalance 360 gm-cm	
Compressor Stage 1 Gap Reduction mm (mils)	0.070	(0.4)	0.53	(20.7)
Compressor Stage 3 Gap Reduction	0.013	(0.5)	0.63	(24.9)
Compressor Stage 5 Gap Reduction	0.013	(0.5)	0.62	(24.6)
Compressor Stage 7 Gap Reduction	0.013	(0.5)	0.64	(25.0)
Support Number 1 Deflection	0.008	(0.3)	0.38	(14.9)
Support Number 2 Deflection	0.005	(0.2)	0.46	(18.3)
Support Number 3 Deflection	0.043	(1.7)	0.12	(4.7)
Case Deflection 1 (Near Front)	0.013	(0.5)	1.06	(41.9)
Case Deflection 2 (Near Bearing Number 2)	0.010	(0.4)	0.50	(19.7)
Case Deflection 3 (Near Bearing Number 3)	0.020	(0.8)	0.53	(21.0)
Case Deflection 4 (Near End)	0.030	(1.2)	2.88	(113.5)
Turbine Stage 1 Gap Reduction	0.043	(1.7)	2.40	(94.5)
Turbine Stage 2 Gap Reduction	0.043	(1.7)	3.33	(131.0)

5.3.3 Military Engine

The curved beam damper was also selected as the most promising concept for the military engine. This engine, which is sensitive to imbalance and support stiffness, was analyzed at various levels of imbalance with the curved beam damper and a conventional squeeze film damper of 0.13 mm (5 mils) radial clearance.

Figure 5.3-5 shows the turbine gap reduction under low 144 gm-cm (2 oz-in), intermediate 1800 gm-cm (25 oz-in), and high 3600 gm-cm (50 oz-in) imbalance loads. At low lvels of imbalance, the turbine gap reductions by conventional damper and curved beam damper were comparable. At high loads, the engine with the proposed damper met safe operating limits, while the conventional damper did not. Even at the intermediate imbalance level, the turbine gap reduction was 3.00 mm (118 mils), which was significantly higher than the limit. As shown in the figure, there is another peak response speed which is just outside the operating range. The gap reduction with the proposed damper slightly exceeded the safety limit at that mode. If that speed proves to be of concern, the damper should be redesigned to attenuate the response. However, since it is beyond the maximum operating speed for an advanced military engine, it is of no concern in this study.

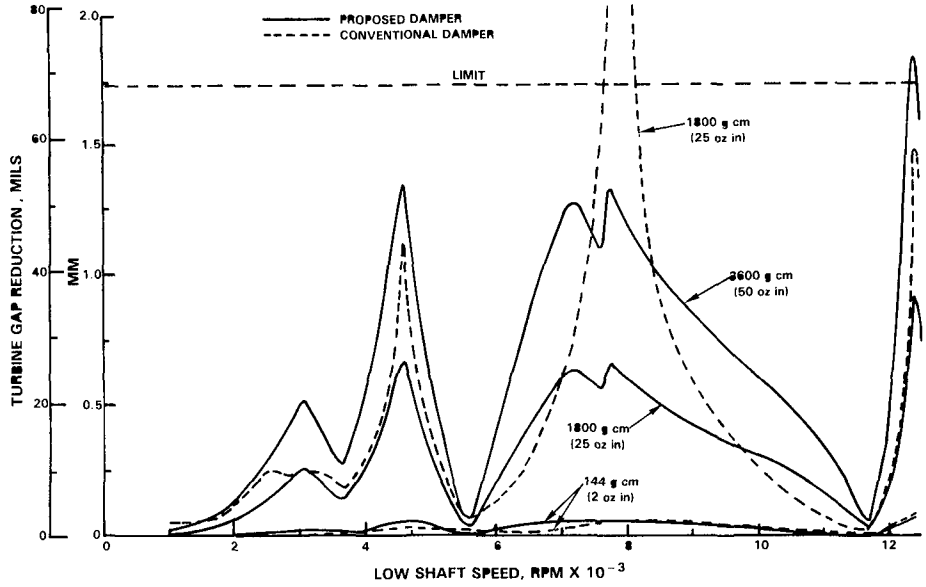

Figure 5.3-5 Turbine Gap Reduction at Low, Intermediate, and High Levels of Imbalance; Conventional and Proposed Dampers; Military Engine

Figure 5.3-6 shows the support load at various levels of imbalance. The proposed damper met the load limit while the conventional damper did not. An intermediate imbalance load of 1800 gm-cm (25 oz-in) produces a bearing load in excess of 45,000 N (10,000LB) the load limit for this engine.

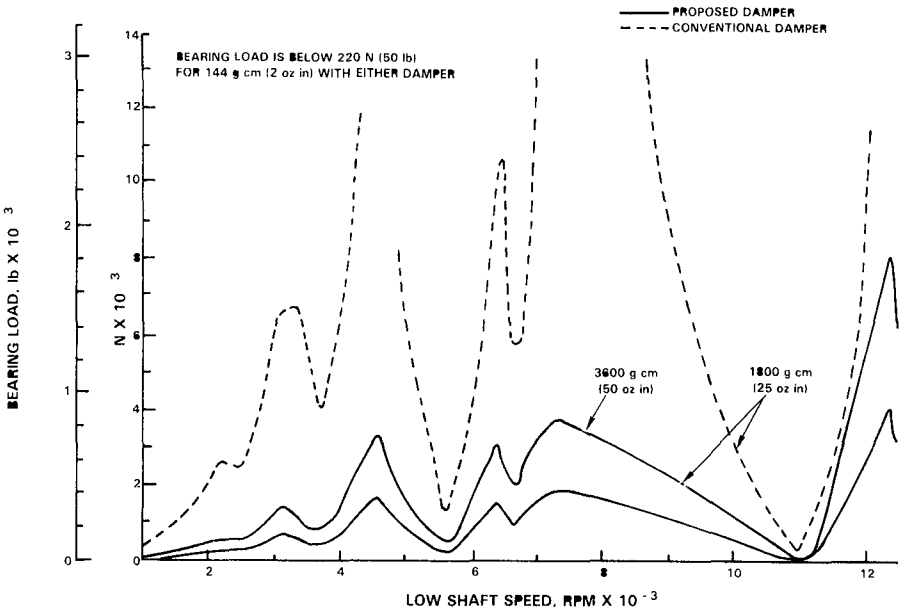

Figure 5.3-6 Number 5 Bearing Loads; Conventional and Proposed Dampers; Military Engine

The overall engine responses with the proposed and conventional dampers are shown in Tables 5.3-V and 5.3-VI. The curved beam damper performed significantly better than the conventional squeeze film damper for intermediate and high imbalance loads.

The response for the curved beam damper at intermediate levels of imbalance can be obtained by linearly scaling the response at low imbalance. This is because the curved beam damper is linear over its operating range.

For conventional squeeze film damper, the engine response exceeded the defined design limits at intermediate levels of imbalance. Therefore the responses at high imbalance loads were not presented.

Table 5.3-V

Military Engine Response; Proposed Damper (Curved beam)

Location	Imbalance 72 gm-cm		3600 gm-cm	
Fan Stage 1 Gap Reduction mm (mils)	0.061	(2.4)	1.52	(60.0)
Fan Stage 2 Gap Reduction	0.041	(1.6)	1.02	(40.0)
Fan Stage 3 Gap Reduction	0.020	(0.8)	0.51	(20.0)
LPT Stage 1 Gap Reduction	0.051	(2.0)	1.27	(50.0)
LPT Stage 2 Gap Reduction	0.051	(2.0)	1.32	(52.0)
Intershaft Gap Reduction	0.091	(3.6)	2.29	(90.0)
Support 1 Deflection	0.003	(0.1)	0.06	(2.5)
Support 2 Deflection	0.015	(0.6)	0.38	(15.0)
Support 3 Deflection	0.036	(1.4)	1.78	(70.0)
Support 4 Deflection	0.005	(0.2)	0.13	(5.0)
Support 5 Deflection	0.023	(0.9)	0.58	(23.0)
Fan Case Deflection	0.036	(1.4)	0.89	(35.0)
Fan Duct Deflection	0.036	(1.4)	0.89	(35.0)

Table 5.3-VI

Military Engine Response; Conventional Damper (0.13 mm squeeze film)

Location	Imbalance 72 gm-cm		1800 gm-cm	
Fan Stage 1 Gap Reduction mm (mils)	0.061	(2.4)	1.34	(52.7)
Fan Stage 2 Gap Reduction	0.036	(1.4)	0.80	(31.5)
Fan Stage 3 Gap Reduction	0.018	(0.7)	0.40	(15.7)
LPT Stage 1 Gap Reduction	0.056	(2.2)	0.38	(14.8)
LPT Stage 2 Gap Reduction	0.053	(2.1)	3.00	(118.0)
Intershaft Gap Reduction	0.076	(3.0)	2.64	(108.0)
Support 1 Deflection	0.003	(0.1)	0.05	(1.9)
Support 2 Deflection	0.013	(0.5)	0.25	(9.8)
Support 3 Deflection	0.041	(1.6)	0.96	(37.7)
Support 4 Deflection	0.005	(0.2)	0.09	(3.5)
Support 5 Deflection	0.020	(0.8)	0.11	(4.2)
Fan Case Deflection	0.033	(1.3)	0.88	(34.8)
Fan Duct Deflection	0.035	(1.2)	0.61	(24)

SECTION 6.0

CONCLUSIONS AND RECOMMENDATIONS

The completion of the work reported herein has added significantly to the understanding of high load damping requirements and the development of damper concepts capable of meeting these requirements. The operational characteristics, relative advantages and disadvantages, and applicability of several concepts was thoroughly investigated in this program. Comparison of engine response with high load dampers and conventional squeeze film dampers led to the following conclusions:

- The proposed damper concepts can be designed to effectively control sensitive vibration modes in modern gas turbine engines subjected to high imbalance loads.

- The curved beam damper showed the greatest potential for successful application to future engines because of its linearity and independent control over stiffness and damping.

- The success of the high load damper concepts was due to their ability to provide required stiffness and damping and allow high excursions without bottoming out.

- Conventional squeeze film dampers designed for normal residual imbalance are too nonlinear to function well under high imbalance load conditions.

Although a substantial enhancement in the understanding of high load dampers has been achieved, additional efforts in this area are required. Each of the damper concepts should be analyzed rigorously under a wide range of operating conditions. More specifically, effort should be directed toward the following objectives:

- The curved beam damper, which showed the most promise for future applications, should be tested experimentally to validate the results of the analysis. Factors which should be considered include fluid inertia, port flow coefficient fluctuation, and the dynamics of the curved beam.

- A more sophisticated analysis of the muti-ring damper should be conducted, focusing on factors such as ring rotation, inertia, and non-identical oil films. In addition, experimental research is required to define the operating characteristics of this damper.

In general, this program expanded the technology base for high load damper concepts. Due to their potential applications in future jet engines, further analytical and experimental efforts are justified.

REFERENCES

1. Feder, E., Bansal, P. N., Blanco, A., "Investigation of Squeeze Film Damper Forces Produced by Circular Centered Orbits," Journal of Engineering for Power, Trans. ASME, January 1978, Volume 100, pp. 15-21.

2. Bansal, P. N., Hibner, D.H., "Experimental and Analytical Investigation of Squeeze Film Bearing Damper Forces Induced by Offset Circular Whirl Orbits," Journal of Mechanical Design, July 1978, Volume 100, pp. 549-557.

3. Marmol, R. A., "Engine Rotor Dynamics, Synchronous and Nonsynchronous Whirl Control," Pratt & Whitney Aircraft Group, Government Products Division, USARTL-TR-79-2, February 1979.

4. Hibner, D.H., Bhat, S. T., Buono, D. F., "Optimum Friction Damping of a Flexible Rotor," ASME Gas Turbine Conference, 1981, Paper Number 81-GT-156.

5. Prohl, M. A., "A General Method for Calculating Critical Speeds of Flexible Rotors," Journal of Applied Mechanics, September 1945, pp. A142-A148.

6. Hibner, D.H., "Dynamic Response of Viscous Damped Multishaft Jet Engines," Journal of Aircraft, Volume 12, Number 4, April 1975, pp. 305-312.

7. Gunter, E. J., Barrett, L. E., Allaire, P. E., "Design of Nonlinear Squeeze Film Dampers for Aircraft Engines," Journal of Lubrication Technology, January 1977, pp. 57-64.

8. Pinkus, V., Sternlicht, B., Theory of Hydrodynamic Lubrication, McGraw Hill, New York, N.Y., 1961.

9. Jones, M. G., "An Experimental Evaluation of Squeeze Film Hydrodynamics," NGTE Report Number 320.

10. Allaire, P. E., Barrett, L.E., Gunter, E. J., "Variational Method for Finite Length Squeeze Film Damper Dynamics with Applications," WEAR 42, 1977, pp. 9-22.

11. Taylor, D. L., Kumar, B. R. K., "Nonlinear Response of Short Squeeze Film Dampers," Journal of Lubrication Technology, Vol. 100, January 1980, pp. 51-58.

12. U. S. Patent Number 4213661, July 22, 1980.

13. Taylor, D. L., Fehr, V. S., "Analysis and Design of Segmented Dampers for Rotor Dynamic Control," Journal of Lubrication Technology, Vol. 104, January 82, pp. 84-90.

NOMENCLATURE

Term	Definition
B	Damping coefficient, lb sec/in, NS/m
C	Radial clearance, in, mm
E	Young's Modulus, lb/in^2, N/m^2
F_R	Radial force, lb, N
F_T	Tangential force, lb, N
K	Stiffness coefficient, lb/in, N/m
L	Axial length, in, cm
N	Number of curved beams
R	Radius, in, cm
Rm	Mean radius, cm
e	Eccentricity, in, cm
l	Half length of curved beam, in, cm
n	Number of films
α	Phase angle between e_1 and e_2, deg
β	Phase angle between e_j and e_2, deg
ϵ	Eccentricity ratio
μ	Viscosity of fluid, Reyns, cp
ω	Whirl speed, rad/sec

Subscripts

eq	Equivalent
f	Friction
j	Journal or shaft
s	Squeeze film
T	Total
1	Film number 1
2	Film number 2

DISTRIBUTION LIST

Contract NAS3-22518

RECIPIENT			NO. OF COPIES
NASA Lewis Research Center 21000 Brookpark Road Cleveland, OH 44135			
Attn:	D. P. Fleming	M.S. 6-1	(20 + reproducible)
	M. J. Hartmann	M.S. 3-7	1
	L. J. Kiraly	M.S. 23-2	1
	D. W. Drier	M.S. 86-2	1
	B. F. Robinson	M.S. 501-11	1
	Library	M.S. 60-3	2
	Report Control Office	M.S. 5-5	2
	Technology Utilization Office	M.S. 7-3	1
	J. Acurio	M.S. 302-2	1
	C. L. Walker	M.S. 302-2	1
	G. J. Weden	M.S. 302-2	1
	J. A. Ziemianski	M.S. 49-6	1
NASA Scientific and Technical Information Facility P. O. Box 8757 Balt./Wash. International Airport Maryland 21240 Attn: Accessioning Department			25
Nasa/Ames Research Center Moffett Field, CA 94035 Attn: Library			1
NASA/Dryden Flight Research Center P. O. Box 273 Edwards, CA 93523 Attn: Library			1
NASA Goddard Space Flght Center Greenbelt, MD 20771 Attn: Library			1
Jet Propulsion Laboratory 4800 Oak Grove Drive Pasadena, CA 91103			1
NASA/Langeley Research Center Hampton, VA 23665 Attn: Library			1

DISTRIBUTION LIST (Cont'd)

RECIPIENT	NO. OF COPIES
NASA/Johnson Space Center Houston. TX 77058 Attn: Library	1
NASA/Marshall Space Flight Ccnter Marshall Space Flight Center, AL 35812 Attn: Library Dr. Otto Goetz MS EP21	1
NASA Headquarters Washington, DC 20546 Attn: RTP-6/R. Colladay RTP-6/J. J. McCarthy	1 1
AVCO-Lycoming 550 S. Main Street Stratford, CT 06497 Attn: M. Saboe Library	1 1
Curtis-Wright Corporation One Passaic Street Woodridge, NJ 07075 Attn: Library	1
Franklin Institute Research Laboratorics 20th & Parkway Philadellhia, PA 19103 Attn: Library Friction & Lubrication Laboratory	1 1
Kaman Aerospace Corporation Old Windsor Road Bloomfield, CT 06002 Attn: Library	1
Marlin Rockwell 402 Chandler Street Jamestown, NY 14701 Attn: Library	1
Mechanical Technology, Inc. 968 Albany-Shaker Road Latham. NY 12110 Attn: Library J. A. Tecza	1 1

DISTRIBUTION LIST (Cont'd)

RECIPIENT	NO. OF COPIES
Pratt & Whitney Aircraft - FRDC P.O. Box 2691 W. Palm Beach, FL 33461	
Attn: V. S. Fehr	1
Library	1
Williams International 2280 W. Maple Road Walled Lake, MI 48088	
Attn: Library	1
Air Force Aero Propulsion Laboratory Wright Patterson AFB, OH 45433	
Attn: AFAPL/SFL/H. F. Jones	1
AFAPL/TBP/L. Gill	1
AFAPL/DO/E. E. Bailey	1
Aerojet-General Corporation 1100 W. Hollyvale Azusa, CA 91702	
Attn: Library	1
Acrospace Corporation P.O. Box 90585 Los Angeles, CA 91745	
Attn: Library	1
Garrett Turbine Engine Company 402 S. 36th Street Phoenix, AZ 85034	
Attn: Library	1
AiResearch Manufacturing Company 9851 Sepulveda Blvd. Los Angeles, CA 90009	
Attn: Library	1
Battelle Columbus Labs. 505 King Avenue Columbus, OH 43201	
Attn: Library	1
Bendix Research Labs. Division Detroit, MI 48232	
Attn: Library	1

DISTRIBUTION LIST (Cont'd)

RECIPIENT	NO. OF COPIES
Boeing Company Aerospace Division P. O. Box 3707 Seattle, WA 98124 Attn: Library	1
Boeing Company Vertol Division, Boeing Center P. O. Box 16858 Philadlphia, PA 19142 Attn: Library	1
General electric Company Aircraft Engine Group 1000 Western avenue Lynn, MA 01910 Attn: R. A. Dangelmaier J. Paladino	1 1
General Electric Company Aircraft Engine Group Cincinnati, Ohio 45215 Attn: A. F. Storace	1
General Electric Company Building 55-219 Schenectady, NY 12345 Attn: E. R. Booser	1
General Electric Company Mechanical Technology Laboratory R&D Center Schenectady, NY 12301 Attn: Library	1
General Motors Corporation Allison Division Indianapolis, IN 46206 Attn: W. H. Parker	1
Hughes Aircraft Corporation Centinda & Teale Avenue Culver City, CA 90230 Attn: Library	1
Institute for defense Analyses 400 Army-Navy Drive Arlington, VA 22202 Attn: Library	1

DISTRIBUTION LIST (Cont'd)

RECIPIENT	NO. OF COPIES
Lockheed Missiles & Space Company P. O. Box 504 Sunnyvale, CA 94088 Attn: Library	1
Massachusetts Institute of Technology Cambridge, MA 02139 Attn: Library	1
National Science Foundation Engineering Division 1800 "G" Street, N. W. Washington, D. C. 20540 Attn: Library	1
Naval Air Systems Command Washington, D. C. 20360 Attn: Library	1
Naval Ship Engineering Center Washington, D. C. 20360 Attn: W. C. Lindstrom NSC 6130B	1
Naval Ship Research & Development Center Annapolis Division Annapolis, MD 21402 Attn: Library	1
Naval Air Propulsion Center Trenton, NJ Attn: R. Valori	1
Rockwell International Rocketdyne Division 6633 Canoga Avenue Canoga Park, CA 91304	1
Office of Naval Research Arlingtn, VA 22217 Attn: S. W. Doroff ONR/438	1
Sundstrand Denver 2480 W. 70th Avenue Denver, CO 80221 Attn: Library	1

DISTRIBUTION LIST (Cont'd)

RECIPIENT	NO. OF COPIES
U. S. Army Engineering R&D Labs. Gas Turbine Test Facility Fort Belvior, VA 22060 Attn: W. Crim	1
University of Akron Department of Mechanical Engineering Akron, OH 44325 Attn: Dr. M. Adams	1
United Technologies Corporation Pratt & Whitney Aircraft Division 400 Main Street East Hartford, CT 06108 Attn: D. H. Hibner Dr. S. T. Bhat D. F. Buono Library	1 25 1 1
United Technologies corporation Sikorsky Aircraft Division Stratford, CT 06497 Attn: L. Burroughs	1
U. S. Army Research & Technology Labs. Fort Eustis, VA 23604 Attn: Library John White	1 1
U. S. Army (AVRADCOM) 4300 Goodfellow Boulevard St. Louis, MO 63120 Attn: E. J. Hollman, DRDAV-QP	1
Southwest Research Institute P. O. Box 28510 San Antonio, TX 78284 Attn: Library Dr. A. J. Smalley	1 1
Northwestern University Department of Mechanical Engineering & Astronautical Science Evanston, IL 60201 Attn: Dr. H. S. Cheng	1

DISTRIBUTION LIST (Cont'd)

RECIPIENT	NO. OF COPIES
Teledyne CAE, Turbine Engines 1330 Laskey Road Toledo, OH 43612 Attn: R. H. Gaylord	1
Ingersoll-Rand Corporation Phillipsburg, NJ 08865 Attn: Mr. P. Kirlan	1
Dr. R. G. Kirk	1
University oif Virginia School of Engineering & Applied Science Charlottesville, VA 22901 Attn: Dr. Edgar J. Gunter	1
Dr. P. E. Allaire	1
Dr. L. E. Barrett	1
The Vibration Institute 101 W. 55th Street, Suite 206 Clarendon Hills, IL 60514 Attn: Dr. R. L. Eshleman	1
Texas A&M University Department of Mechanical Engineering College Station, TX 77843 Attn: Dr. J. M. Vance	1
Dr. D. W. Childs	1
Cornell University Department of Mechanical Engineering Ithaca, NY 14853 Attn: Dr. D. L. Taylor	1
Arizona State University Department of Mechanical Engineering Attn: Dr. H. D. Nelson	1
Army Research Office P. O. Box 12211 Research Triangle Park, NC 27709	1
Mr. D. E. Bently President Bently Nevada Corporation Box 157 Minden, NV 89423	1

DISTRIBUTION LIST (Cont'd)

RECIPIENT	NO. OF COPIES
Mr. P. Bernhard Manager - OEM Accounts IRD Mechanalysis, Inc. 6150 Huntley Rd. Columbus, OH 43229	1
Mr. J. B. Catlin Manager - Applications Engineer IRD Mechanalysis, Inc. 6150 Huntley Rd. Columbus, OH 43229	1
Mr. G. H. Thomas IRD Mechanalysis, Inc. 6150 Huntley Rd. Columbus, OH 43229	1
Mr. T. Bond Advanced Engineering & Development Turbodyne Corporation 37 Coats St. Wellsville, NY 14985	1
Mr. C. E. Beiser Monsanto Company 800 North Lindbergh Blvd. St. Louis, MO 163166	1
Mr. M. Botman Engineering Structures & Dynamics United Technologies of Canada, Ltd. P. O. Box 10 Longueuil, Montreal 23, Quebec Canada	1
Dr. J. A. Dopkin Supervising Eng. Solid Mechanics Ingersoll-Rand Company Research Center Princeton, NJ 08540	1
Dr. M. F. Giberson Turbo Research, Inc. 1440 Phoenixville Pike West Chester, PA 19380	1

DISTRIBUTION LIST (Cont'd)

RECIPIENT	NO. OF COPIES
Dr. E. J. Hahn Dept. of Mechanical Engineering University of New South Wales Sydney, Australia	1
Mr. J. Halloran Chief Engineer Joy Manufacturing Company P. O. Box 209 3101 Broadway Buffalo, NY 14225	1
Mr. G. K. Mruk Analytical Engineer Joy Manufacturing Company P. O. Box 209 3101 Broadway Buffalo, NY 14225	1
Mr. B. Herbage President Centritech Corporation 9919 Steelman Avenue Houston, TX 77017	1
Mr. C. Jackson Monsanto Company P. O. Box 1311 Texas City, TX 77590	1
Mr. W. Jogwick Union Carbode Corporation P. O. Box 8361 South Charleston, WV 25303	1
Mr. A. Rod Structural Dynamics Research Corp. 5729 Dragon Way Cincinnati, OH 45227	1
Dr. C. Bert University of Oklahoma 1928 Goddard, North Campus Norman, OK 73069	1

DISTRIBUTION LIST (Cont'd)

RECIPIENT	NO. OF COPIES
Mr. A. Royal U. S. Army R&D Laboratory Eustis Directorate Fort Ustis, VA 23604	1
Mr. H. Tripp Shell Development Company P. O. Box 481 Houston, TX 77001	1
Mr. B. Johnson United Technologies Research Center Silver Lane Est Hartford, CT 06108	1
Dr. K. Maurer Mechanical Engineering Dept. North akota State University Fargo, ND	
Dr. L. D. Mitchell Mechanical Engineering Dept. Virginia Polytechnic Institute & State Univ. Blacksburg, VA 24060	1
Dr. R. Pendleton South Dakota School of Mines & Technology CM 103 Rapid City, SD	1